Single-Walled Carbon Nanotube Fluorescent Sensors for Monitoring the Activity and Inhibition of Cholinesterase Enzymes

Dan Loewenthal
The Raymond and Beverly Sackler Faculty of Exact Sciences,
School of Chemistry
Tel Aviv University

A thesis submitted toward the degree of
Master of Science in Physical Chemistry

October, 2022

Single-Walled Carbon Nanotube Fluorescent Sensors for Monitoring the Activity and Inhibition of Cholinesterase Enzymes

Dan Loewenthal

The Raymond and Beverly Sackler Faculty of Exact Sciences,

School of Chemistry

Tel Aviv University

A thesis submitted toward the degree of

Master of Science in Physical Chemistry

October, 2022

This research was carried out in the Department of Biomedical Engineering. Under the Supervision of Dr. Gili Bisker

Acknowledgments

First and foremost, I would like to thank my supervisor Dr. Gili Bisker. Gili had the courage to allow me to pursue this project despite myself being a rather unusual student, working full-time in parallel at IIBR. Gili's scientific leadership throughout the project, her priceless comments on writing papers, grants and preparing figures, and her talent for project and team management are invaluable lessons that I will hold close to my heart for the rest of my scientific journey. Thank you so much.

I would also like to thank my lab members, specifically Dr. Adi Hendler-Neumark, Dr. Verena Wulf, Eddie Shraga and Dr. Dotan Kamber for their comments throughout this project and their support. This could not have been done without you.

I want to thank my friends and colleagues at IIBR for their extreme open - mindedness and flexibility in allowing me to pursue this project, encouraging me and hearing my thoughts during the project. I would specifically like to single out Dr. Shai Dagan and Dr. Sigalit Gura for their belief in me and their help in organizing everything so that this project could be done. Also, originally from IIBR, I would like thank Dr. Gabriel Amitai for exciting talks early in the project and all his encouragement throughout it. I will always hold IIBR to the highest regard for its excellent science, and moreover the excellent people.

Lastly, I would like to thank my family. My mother, father, and my sister: Limor, Ron and May. Whether it is delivering snacks so I can continue studying, sharing my excitement with you at the end of the day about an experiment that worked, or your never-ending encouragement and help, thank you for all these things, small to large, which are the fruitful soil on which I am lucky enough to flower. With a loving heart, and a head high for the adventures to come, thank you.

Abstract

Cholinesterase enzymes are involved in a wide range of bodily functions, and their disruption is linked to pathologies such as neurodegenerative diseases and cancer. While cholinesterase inhibitors are used as drug treatments for diseases such as Alzheimer and dementia at therapeutic doses, acute exposure to high doses, found in pesticides and nerve agents, can be lethal. Therefore, measuring cholinesterase activity is important for numerous applications ranging from the search for novel treatments for neurodegenerative disorders to the on-site detection of potential health hazards. Here, we present the development of a near-infrared (near-IR) fluorescent single-walled carbon nanotube (SWCNT) optical sensor for cholinesterase activity and demonstrate the detection of both acetylcholinesterase and butyrylcholinesterase, as well as their inhibition. We show sub U L-1 sensitivity, demonstrate the optical response at the level of individual nanosensors, and showcase an optical signal output in the 900-1400 nm range, which overlaps with the biological transparency window. To the best of our knowledge, this is the longest wavelength cholinesterase activity sensor reported to date. Our near-IR fluorescence-based approach opens new avenues for spatiotemporal-resolved detection of cholinesterase activity, with numerous applications such as advancing the research of the cholinergic system, detecting on-site potential health hazards, and measuring biomarkers in real time.

Publication

Dan Loewenthal, Dotan Kamber, Gili Bisker, "**Monitoring the Activity and Inhibition of Cholinesterase Enzymes Using Single-Walled Carbon Nanotube Fluorescent Sensors"**, *Anal. Chem. 2022, 94 (41), 14223-14231*

Table of Contents

List of Figures

Introduction

Cholinesterase Enzymes and their measurement

Cholinesterase (ChE) enzymes hydrolyze choline esters in the body and are linked with a diverse range of bodily functions and pathologies. Acetylcholinesterase (AChE) is found mainly at neuronal synapses, where it modulates neuronal transmission via hydrolysis of acetylcholine. Disruption of AChE has been linked with pathologies such as Alzheimer's disease, Parkinson's disease, Myasthenia Gravis, Depression, Organophosphorus poisoning and cancer[1–4] .

Acetylcholinesterase exists in various forms, two of the important ones are the tetrameric amphiphilic membrane-bound form found in vertebrate brains and the hydrophilic water soluble tetrameric form found in various cell secretions, cerebrospinal fluid, and in blood[5].

Butyrylcholinesterase (BChE) is a less specific ChE enzyme, found mainly in the plasma, and its disruption has been linked with sudden infant death syndrome and Alzheimer's disease, potentially serving as a biomarker[6,7]. Over the years, it has mainly been studied due to its hydrolytic action of succinylcholine, a muscle relaxant, in which mutated forms of BChE in certain individuals cause prolonged apnea in some succinylcholine treated anesthetized patients. BChE exists mainly as its tetrameric form, with two subunits bound by a disulfide bond associated with two other subunits by hydrophobic interactions[5] (Figure 1).

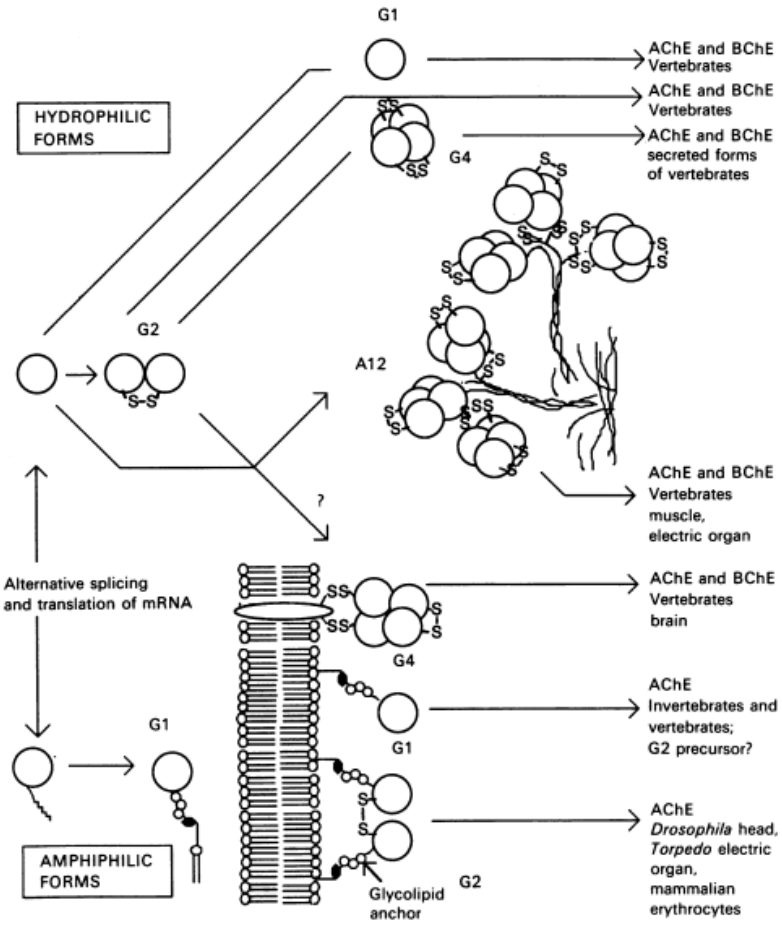

Figure 1: Cholinesterase enzymes polymorphisms. Cholinesterase enzymes exist in amphiphilic and hydrophilic forms, each of the forms has multiple possible quaternary structures. Adapted from [5].

The mechanism of synaptic AChE activity is as briefly as follows (Figure 2): an action potential stimulates acetylcholine release into a cholinergic synapse, acetylcholine then binds to an acetylcholine receptor, triggering a cascade of reactions which eventually sensitize the membrane for propagation of the action potential or muscle contraction, AChE then hydrolyses acetylcholine, terminating the signal.

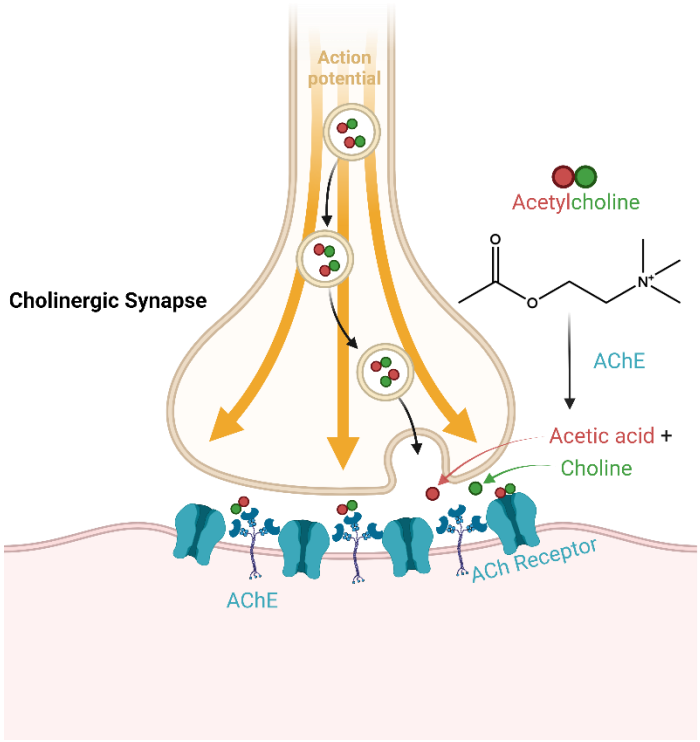

Figure 2: Diagram of a cholinergic synapse. The drawing showcases the process of action potential-triggered acetylcholine release, binding to acetylcholine (ACh) receptors followed by acetylcholinesterase mediated hydrolysis.

Interestingly, the catalytic activity of AChE is extremely fast, with a turn over rate larger than $10^8 M^{-1} s^{-1}$, approaching diffusion limited catalysis[8]

While cholinesterase inhibitors can serve as therapeutics, high doses found in organophosphate, pesticides, and nerve agent, cause cognitive decline and mortality[9]. Therefore, measuring the activity of these enzymes is important for the detection of health-hazards, biomarker monitoring, studies of the cholinergic system, and the search for novel therapeutics for neurodegenerative diseases.

Traditionally, ChE activity is measured by the Ellman absorbance-based assay[10] (Figure 3), in which acetylthiocholine is hydrolyzed by a cholinesterase to produce thiocholine, which subsequently reacts with 5,5′-dithiobis-(2-nitrobenzoic acid) to produce a yellow color, which can be measured using absorbance spectroscopy. This approach, however, only measures average quantities (bulk) and is limited in its optical selectivity compared to fluorescent methods.

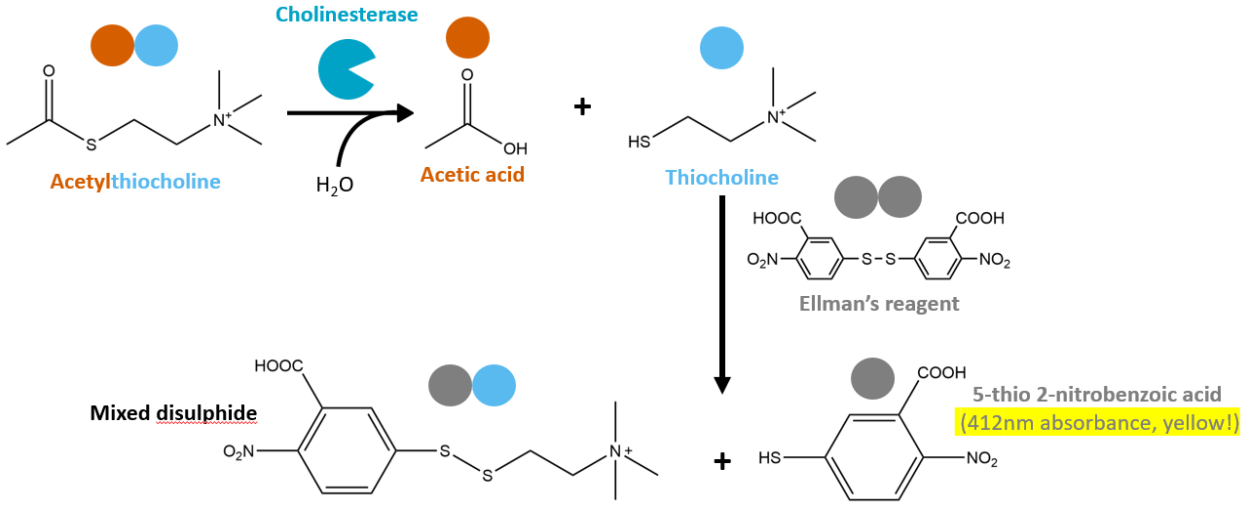

Figure 3: "Ellman" absorbance assay for the quantification of cholinesterase activity. Acetylthiocholine is hydrolyzed by a cholinesterase enzyme to produce acetic acid and thiocholine. Subsequently, thiocholine reacts with Ellman's reagent to produced a mixed disulfide and 5-thio 2-nitrobenzoic acid which absorbs in 412nm, allowing quantification of the produced thiocholine and thus enzymatic activity.

Over the last few years, many research efforts focused on developing fluorescent nanosensors for ChE activity and inhibition[11,12,21,13–20], some of which were able to provide spatiotemporal resolution[12–14,19]. Fluorescent sensors hold promise for superior optical selectivity over the more traditional absorbance-based methods when measuring in the presence of biological media[10,22,23], while spatiotemporal-resolving sensors offer exciting possibilities over the more traditional bulk measurements. For example, such spatiotemporal information can potentially serve as tumor resection guides due to cholinesterase activity difference between brain

glioma cells and normal brain cells[12]. However, many of these new methods involve complex cascade reactions or experimental setups, and their optical outputs are usually up to 800 nm at most, limiting tissue penetration and the signal-to-noise ratio due to tissue autofluorescence[24–26].

Single-Walled Carbon Nanotubes (SWCNTs)

Single walled carbon nanotubes can be theoretically thought of as "rolled" graphene sheets. As such, they are effectively a one-dimensional material, with a typical width of 0.4-10 nm and a two\three orders of magnitude larger length. Sometimes grown to sizes of several centimeters[27].

Single walled carbon nanotube species can be characterized by their "chirality" which essentially specifies a rolling vector to the theoretical "rolled" up graphene sheet[28]. This roll-up vector is composed of a_1 and a_2 basis vectors (illustrated in the figure) as $\vec{c} = n\,\overrightarrow{a_1} + m\,\overrightarrow{a_2}$, and specifies nodes on which the theoretical graphene sheet would be rolled over to produce a given SWCNT long-range crystalline order. As such, it defines both the chirality and diameter of SWCNT species. For example, Figure 4 illustrates the theoretical rolling of a graphene sheet to produce a (6,5) chirality SWCNT.

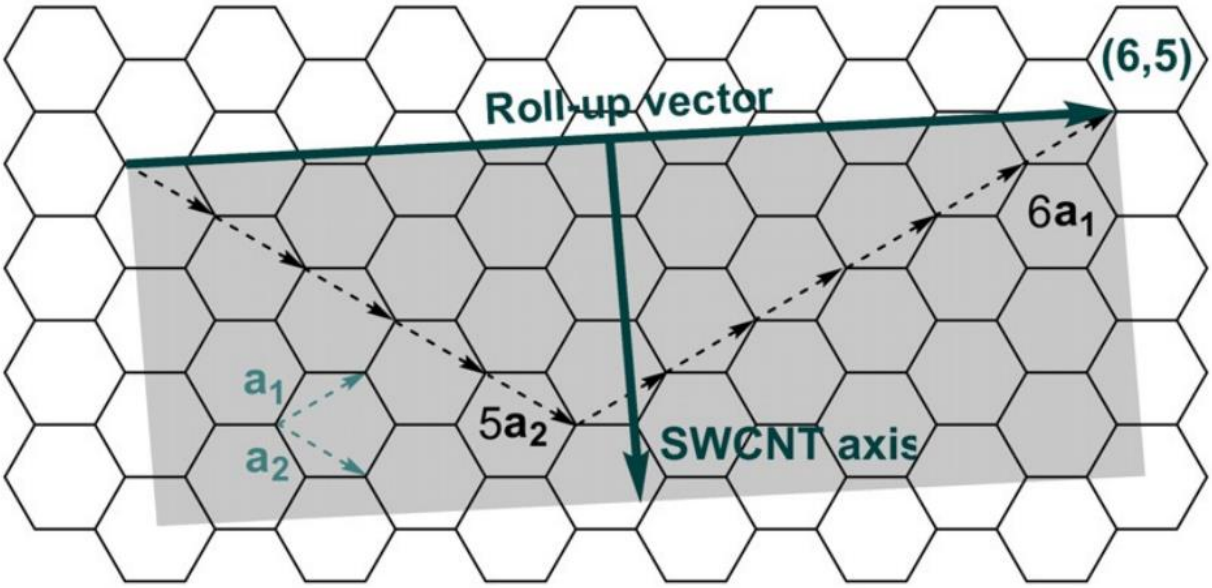

Figure 4: Diagram for the roll up vector specifying nanotube chirality. The roll up vector is composed of two basis vectors a_1 and a_2 along the hexagonal lattice which specify a direction for the theoretical graphene sheet to "roll" in order to prduce the specified crystalline SWCNT lattice. Adapted from[28] .

Note that when the n and m vector coefficients are different, (n, m) and (m, n) the two SWCNT species are enantiomers, as these can correspond to rolling the sheet "into" and "out of" the two-dimensional plane, resulting in two different species which are non-overlapping mirror images of each other. Recently, enantiomeric SWCNT species were demonstrated to have different interactions with chiral analytes[29].

As SWCNT chirality determines the crystalline order of the sp2 hybridized carbon atoms in the SWCNT, it affects the density and energy of the electronic states as well as their physical and chemical properties. As a quick summary, when $n - m = 0$ SWCNTs are metallic (armchair configurations), when $n - m = 3j$ $(j \in N \backslash \{0\})$ SWCNTs are semi-metallic and have a small band gap $(1 - 100\ [meV])$, and for all other n, m configurations they are semiconducting and show a large band gap $(0.5 - 1\ [eV])$[27] (Figure 5).

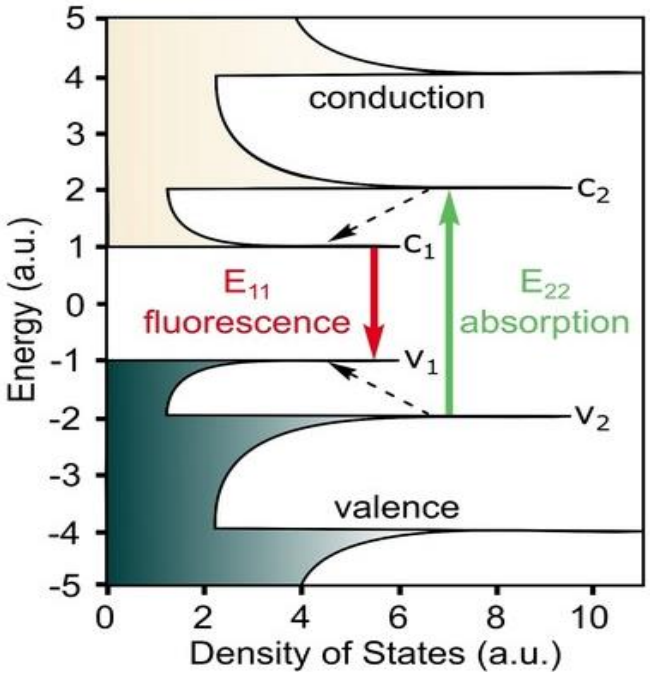

Figure 5: Band gap structure of semi-metallic single walled carbon nanotubes. Absorbance usually excites valence electrons to the second conduction band, followed by relaxation to the first conduction band and a fluorescent radiative transition in the near IR range. Adapted from[28]

Semiconducting SWCNTs can thus be illuminated with light to create electron-hole excitons which diffuse along the SWCNT axis[30–32]. The exciton size is about 2 nm and diffuses ~100 nm[31,33,34]. These excitations excite electrons usually to the second conductance band with a femtosecond decay to the first conductance band followed by fluorescent radiative transition in the near IR range[31,32,35] (Figure 6).

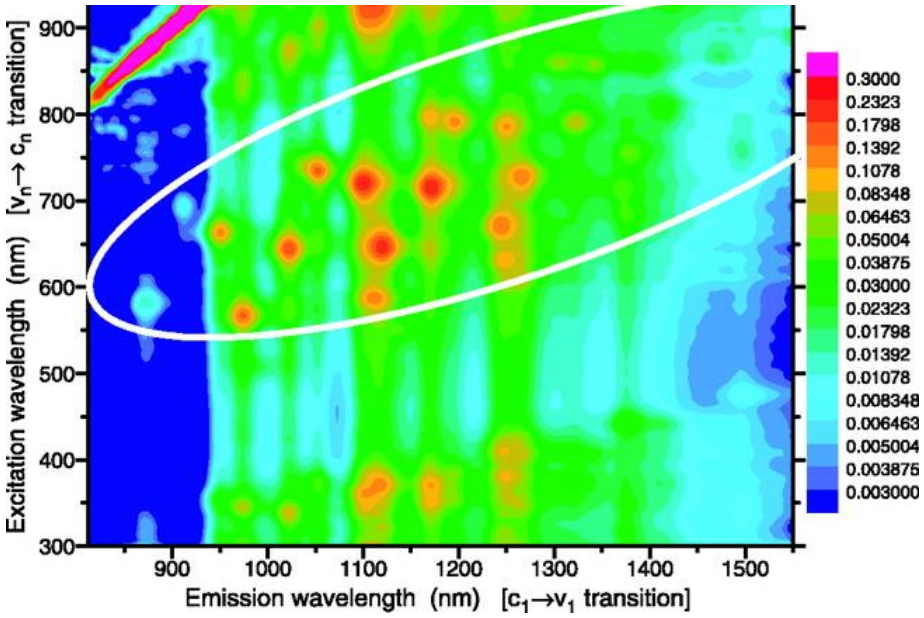

Figure 7: SWCNT fluorescence excitation emission plot. Each single walled carbon nanotube chirality corresponds to a different excitation emission wavelength pair (seen as a red dot). As such, fluorescent response can be allocated to SWCNT chirality. Adapted from[32]

This optical range is especially attractive for biomedical application as it overlaps with the biological transparency window, where biological samples show little to none optical activity[36–43]. Moreover, SWCNT sensors are stable at room temperature, provide spatiotemporal information, and do not photobleach upon use, unlike many other fluorescent sensors[44–47].

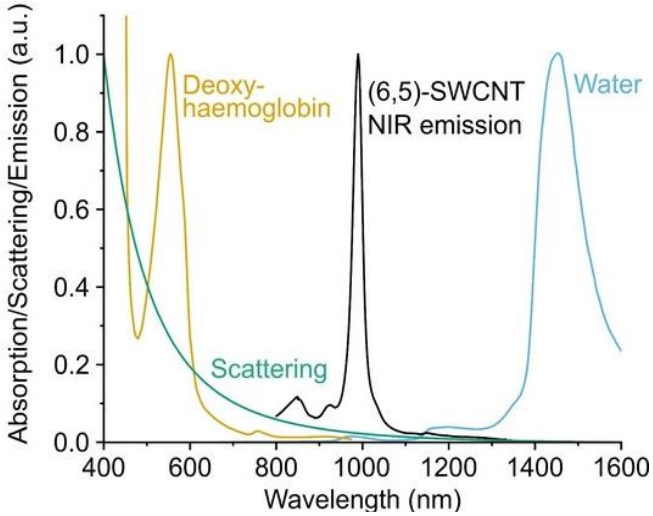

Figure 6: SWCNT emission in the near IR biological transparency window. It is easy to see that the fluorescent emission of SWCNTs is in a wavelength for which there is little biological optical activity. Adapted from [28]

As excitons travel along the surface of SWCNTs[30], they are highly sensitive to surface effects thus making the photophysical response of SWCNTs sensitive to their surroundings, also paving the path to their use as fluorescent sensors.

However, due to extensive pi interactions SWCNTs are hydrophobic and will aggregate in water, quenching their fluorescence. As such, one must suspend these SWCNTs using other chemicals to maintain their fluorescence in solution. But this curse can also be a blessing: As these suspensions mediate the response of SWCNTs to their surrounding in a selective manner, dependent on the suspension design used, they render chemical selectivity to the fluorescent response[44,48].

Single-Walled Carbon Nanotube Fluorescent Sensors

Now, armed with the knowledge of photophysics of SWCNTs, one can start designing suspensions that render chemical selectivity to desired analytes. The two main approaches are as follows: rational design, and screening approaches.

In rational design approaches, SWCNTs are rendered selective to analytes through a certain classical chemical recognition motif. This could be an antibody, an aptamer, or even an enzymatic substrate if our "analyte" is an enzyme[49]. Screening based approaches usually rely on permutations of lipids, DNA or RNA to screen for a chemical sequence that renders selectivity for a certain analyte. For non-covalent suspensions, usually the suspending chemicals are amphiphilic, with an hydrophobic anchor point and hydrophilic sequence which stabilizes the suspension and forms a binding site for the analyte[44]. These are introduced above the critical micelle concentration thus forming stable colloidal suspensions (Figure 8).

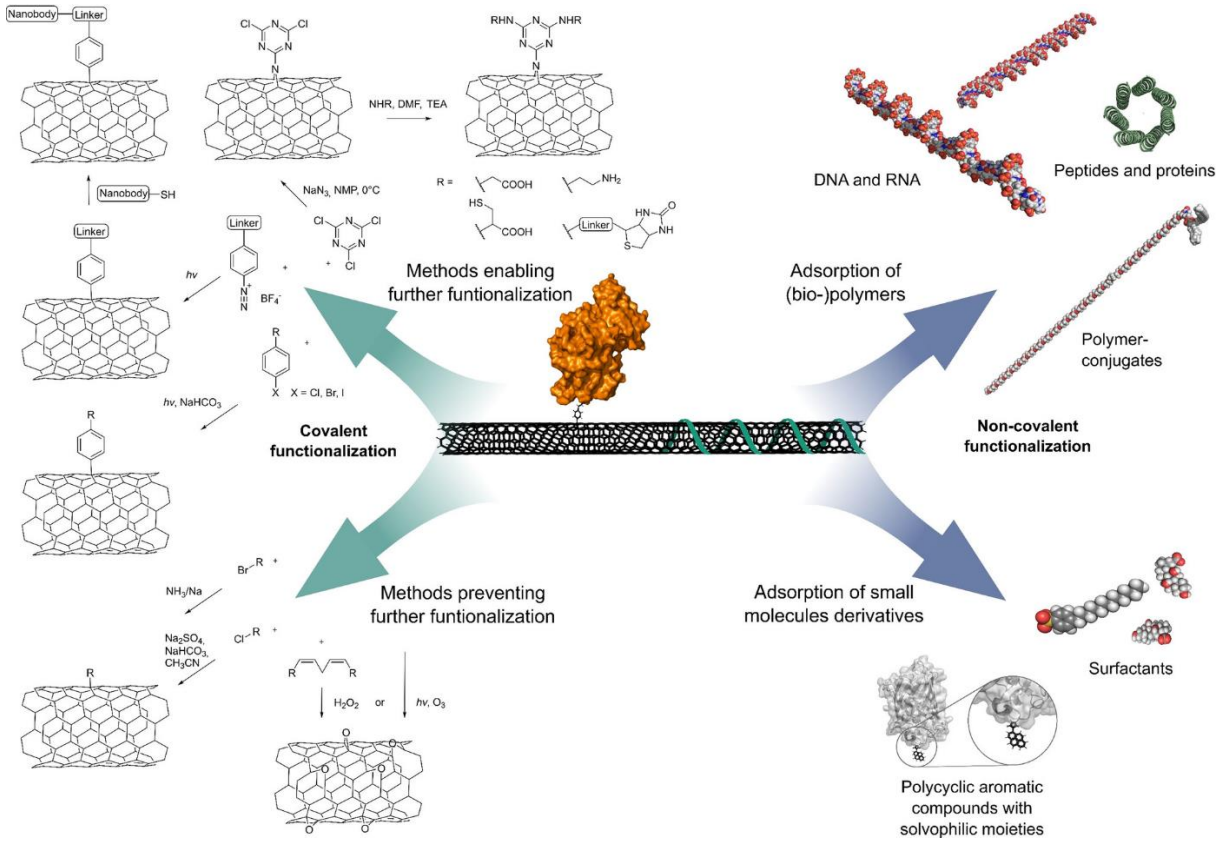

Figure 8: SWCNT suspension and functionalization approaches. Notice the different between covalent (left) and non covalent (right) functionalization of SWCNTs for their use as sensors. Adapted from [28] .

In both screening and rational design approaches, a certain change in the dielectric environment around the SWCNT would yield a change in fluorescence. This might be manifested in a change in fluorescence intensity, a shift in fluorescence wavelength, or even both.

Current scientific literature proposes a variety of mechanisms for fluorescence modulation mediated by phases around the SWCNT upon interaction with analytes (Figure 9). Briefly, these include direct exciton quenching by the analyte, conformational change of the suspension directly through the analyte or through changes in functional groups, and solvation\ion distribution effects upon introduction of the analyte. With such diverse supramolecular mechanisms, this is

an active area of research which offers promise for improved design of SWCNT based sensors.

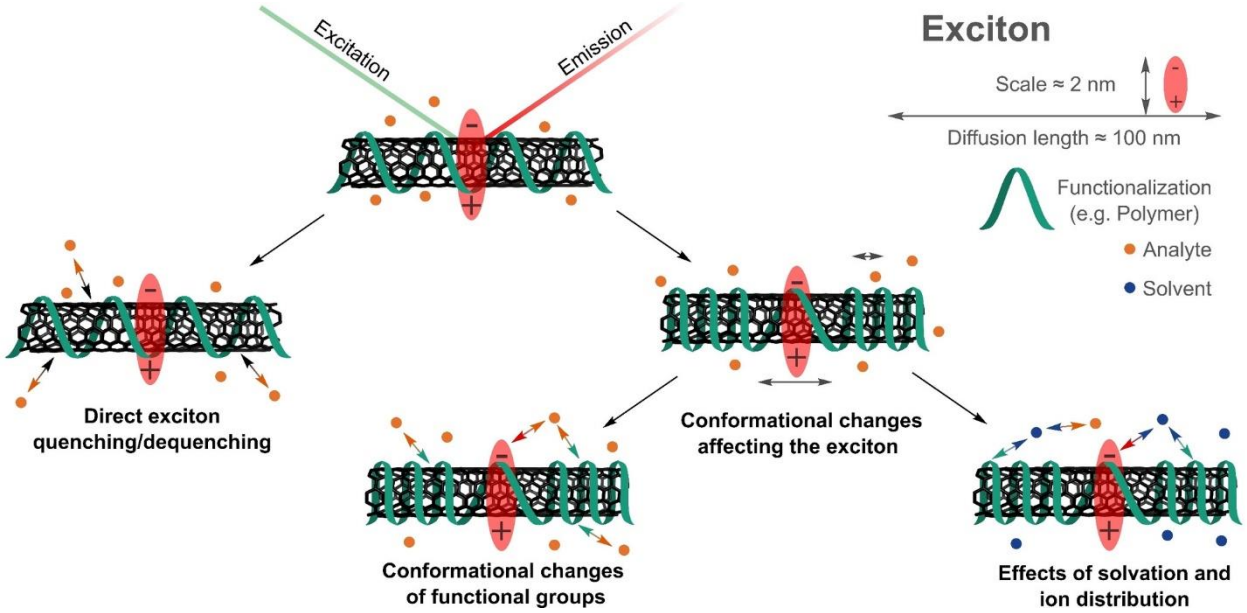

Figure 9: Fluorescence modulation mechanisms for SWCNT-analyte interactions. Introduction of analyte can cause direct fluorescence quenching/dequenching or a conformational change which affects fluorescent activity. Adapted from [28]

In this example (Figure 10), one can see a library screening of lipids and ssDNA suspensions in order to find a protein targeted SWCNT sensor. Here, a strong and selective response to Fibrinogen was clearly demonstrated for the $(AT)_{30}$ ssDNA sequence[48].

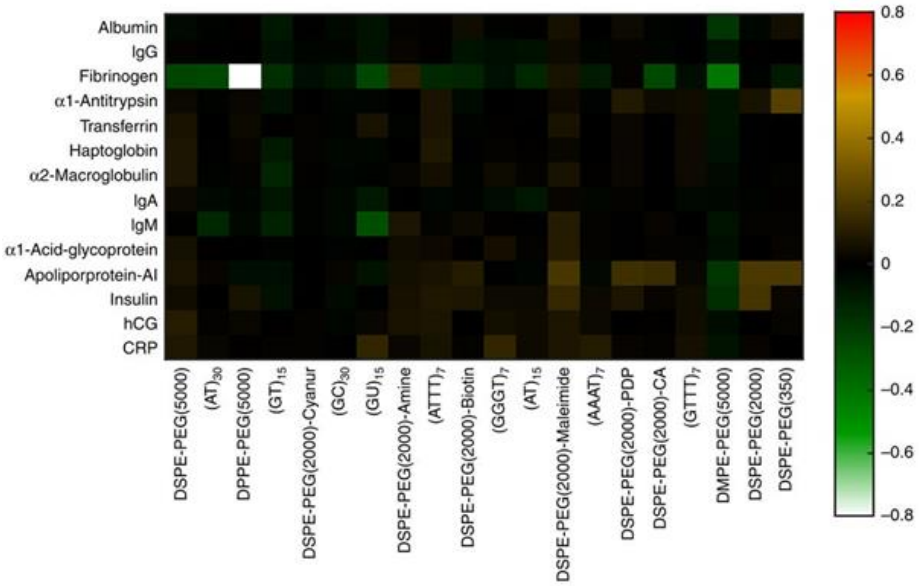

Figure 10: SWCNT screening assay for protein analytes. A selective fluorescent response can be clearly seen for $(AT)_{30}$ ssDNA coated sensor to fibrinogen. Adapted from[48]

Fluorescent SWCNT sensors were applied for the biosensing of different analytes and enzymes[28,38,55–58,40,47,48,50–54]. These range from monitoring progresetrol and cortisol *in vivo* (mice)[40], fibrinogen and insulin in blood and cell culture[48,50], nitroaromatics[38] and pathogens[54,59,60] *in vivo* (plants), volatiles in gaseous phase[61,62], to enzymatic activity[49,63,64].

Specifically for enzymatic sensing, recent works include designing dendrons as tailorable suspensions enzymatic activity analysis[49], development of a reporter of an enzymatic suicide inactivation pathway[63], and detection of protease activity using peptide-encapsulated SWCNTs[61].

Project Outline

Here, we present a sensitive, near-IR, SWCNT fluorescent nanosensor for ChE activity and inhibition[65]. The sensor is based on selective recognition of thiocholine, the cholinesterase-hydrolysis product of acetylthiocholine, triggering a near-IR fluorescence intensity increase of DNA-functionalized SWCNTs (Figure 11). We elucidate the recognition mechanism, demonstrate an optical output in the 900-1400 nm range, find a sub U L^{-1} limit of detection, demonstrate the ability to infer BChE inhibition, and lastly resolve the fluorescence response to enzymatic activity at the single-nanosensor level with spatiotemporal information.

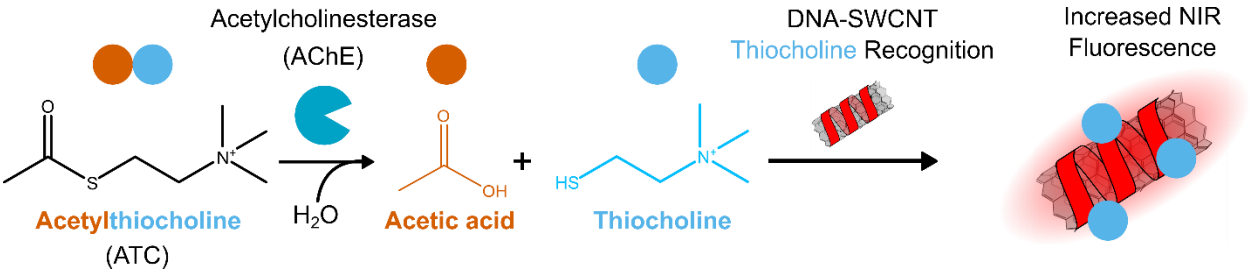

Figure 11: AChE activity sensing mechanism. AChE hydrolyses acetylthiocholine to acetic acid and thiocholine; thiocholine is then recognized by a DNA-SWCNT sensor resulting in increased near-IR fluorescence intensity.

Methods

DNA-SWCNTs suspension

1 mg of HipCO SWCNTs and 2 mg DNA in 0.1M NaCl were bath sonicated (Elma P-30H) for 10 minutes at 80 Hz and tip-sonicated twice (Qsonice Q125, 3 mm tip, 4 W) for 20 minutes in an ice bath. The suspension was centrifuged twice at 16,100 rcf for 90 minutes, where after each centrifugation step, 80% of the supernatant was collected and the rest discarded. The resulting DNA-SWCNT concentration was measured by absorbance spectroscopy (Shimadzu UV-3600 Plus)[45,66] using an extinction coefficient[45] of $\varepsilon_{632\,nm} = 0.036$ L mg^{-1} cm^{-1}.

The DNA oligomers screened were (5' to 3'): $(GT)_{15}$, $(TAT)_4$, $(GTTT)_7$ $(GC)_{30}$, and $(T)_{30}$.

Near-IR fluorescence spectroscopy of DNA-SWCNTs

The fluorescence intensity of the DNA-SWCNT samples was measured on a near-IR inverted fluorescence microscope (Olympus IX73). A 730 nm continuous-wave laser (MDL-MD-730-1.5W, Changchun New Industries) was used for excitation and a near-IR spectrometer (Spectra Pro HRS-300, Princeton Instruments) with a slit-width of 500 μm and a grating of 150 g/mm coupled to an InGaAs line detector (PylonIR, Teledyne Princeton Instruments) was used for spectrally resolved fluorescence detection, with a 1 s exposure time.

DNA- SWCNTs excitation-emission spectra

DNA-SWCNTs were diluted to 1 mg L^{-1} in PBS pH 7.4 and were illuminated with a super-continuum white-light laser (NKT-photonics, Super-K Extreme) with a bandwidth filter (NKT-photonics, Varia, $\Delta\lambda = 20$ nm) scanned between 500-840 nm with an excitation time of 2 s per wavelength, a 1 nm wavelength step size and 20 mW (at 730 nm) intensity. Emission spectra were recorded using the near-IR

spectrometer described above. Spectra were background subtracted of a phosphate buffered saline (PBS, pH 7.4) sample and can be found in the appendix (Figure S1).

Screening DNA-SWCNT library for AChE-responsive sensors

For each sensor, 147 µL of 1 mg L^{-1} DNA-SWCNT suspension in PBS was spiked with 3 µL of 5 mM acetylthiocholine (0.1 mM acetylthiocholine in the resulting solution) or 3 µL of PBS as control and the fluorescence response was recorded after one hour. Subsequently, samples that contained acetylthiocholine were spiked with AChE (3 µL, 10 U L^{-1} in the resulting solution), and the fluorescence response was recorded after one hour. Data are presented as the normalized fluorescence intensity of the (9,4) DNA-SWCNT chirality.

DNA-SWCNT fluorescence response kinetics and limit of detection for AChE\BChE

147 µL of SWCNTs solution (1 mg L^{-1} in PBS pH 7.4) were spiked with 3 µL of 5 mM acetylthiocholine and incubated for 10 minutes to ensure stabilization. Afterward, 3 µL of the enzymes at different U L^{-1} activity were spiked to the SWCNTs solution and the fluorescence spectra dynamics were monitored for two hours with the near-IR inverted fluorescence microscope. The limit of detection (LOD) was calculated as the concentration at which the signal is three times the standard deviation of the noise level. Data are presented as the normalized fluorescence intensity of the (9,4) DNA-SWCNT chirality. Enzyme quantity is presented in U, which is the amount of enzyme that hydrolyses 1 micromole of acetylthiocholine per minute at room temperature and pH 7.5. All error bars represent the standard deviation of experimental replicates.

Sensor response kinetics and concentration dependence to relevant small molecules

147 µL of SWCNTs solution (1 mg L^{-1} in PBS pH 7.4) were spiked with 3 µL of cysteine, acetylthiocholine, choline, and acetic acid for final concentrations of 10, 100, 300, 1000 µM. 3µL of Neostigmine was spiked for final concentrations of 1,10,30,100 µM. Data are presented as the normalized fluorescence intensity of the (9,4) DNA-SWCNT chirality. Samples were measured in triplicate and the fluorescence intensity was monitored with time. Signals were normalized to the first time point.

BChE inhibition assay

147 µL of DNA-SWCNTs solutions (1 mg L^{-1} in PBS pH 7.4) were spiked with 3 µL of Neostigmine (100 mM) and 3 µL of 0.5 U L^{-1} BChE solution in PBS pH 7.4 and stirred gently at room temperature for 10 minutes for cholinesterase inhibition. Subsequently, 3 µL of acetylthiocholine (5 mM) were spiked for a final concentration of 100 µM in solution and the fluorescence response was monitored for one hour. Signals were normalized to the fluorescence intensity before the addition of acetylthiocholine. Data are presented as the normalized fluorescence intensity of the (9,4) DNA-SWCNT chirality.

Ellman Assay

The assay is based on a well-established protocol[22]. Briefly, diluted samples were incubated with 5,5-dithio-bis-(2-nitrobenzoic acid) at 37°C for 10 minutes, to which acetylthiocholine was added to a final concentration of 0.45 mM in solution. Immediately after acetylthiocholine addition, sample absorbance was recorded at 436 nm for 3 minutes using a plate reader (Fusion Optics Reader Platform SPARK). The resulting linear absorption over time curve is a direct indication of the amount of 3-carboxy-4-nitrobenzenethiolate (ε = 10.6×103 M^{-1} cm^{-1}) anion formed, which

itself is in direct proportion to the amount of thiocholine formed in solution and thus ChE activity.

Cholinesterase activity measurement in serum

Fetal bovine serum (Sigma) was diluted in PBS in the range of 1:30 to 1:300 and the cholinesterase activity of each dilution was quantified with the Ellman assay. (GT)15-SWCNTs were incubated at 1 mg L-1 in the diluted serum solution for two hours. 147 µL of the (GT)15-SWCNT in serum solution were spiked with 3 µL acetylthiocholine (22.5 mM stock concentration) for a final concentration of 450 µM, and the fluorescence intensity was monitored for 12 minutes. Signals were normalized to the fluorescence intensity at the beginning of the assay and compared to control samples of the same serum dilution to which no acetylthiocholine was added (Figure S5). Data are present-ed as the background-subtracted, normalized fluorescence intensity of the (9,4) SWCNT chirality.

Fluorescence imaging

For enzyme activity imaging, an 18 *mm* × 18 *mm* glass coverslip was rinsed with water and EtOH, and left to dry. 300 µL of 0.01% Poly-L-Lysine solution in water was pipetted onto each slide. After 15 minutes, the slides were washed with water and dried with a stream of nitrogen. 300 µL of 1 mg L^{-1} $(GT)_{15}$-SWCNT solution in water was added to each well for 15 minutes incubation, followed by a washing step with water and drying with a stream of nitrogen. Coverslips were then adhered to a plastic slide with a built-in well (Chroma Technology Corp). 300 µL of acetylthiocholine (450 µM) in PBS were added to the well. After two minutes, 5 µL of diluted BChE solution were spiked into the well, and the fluorescence response over time was recorded. For thiocholine imaging, 200 µL PBS were added to the coverslip well followed by 100 µL of thiocholine solution (1.35 mM) for a final

concentration of 450 μM thiocholine and the fluorescence intensity change upon addition was recorded.

Images were taken with an inverted fluorescence microscope (Olympus IX83) at 100× magnification (100x 1,3NA, Plan FL objective), operated in highly inclined and laminated optical sheet (HiLo) microscopy mode[67], to minimize the illumination depth compared to epi-fluorescence. Fluorescent samples were excited with a 730 nm continuous-wave laser (MDL-MD-730-1.5W, Changchun New Industries) at approximately ~440 mW (20 W mm^{-2}*)*, and the near-IR emission was imaged after a 900 nm long-pass emission filter (Chroma ET900lp) with a cooled InGaAs-camera (Raptor, Ninox-640 VIS-NIR). Videos were taken at a frame rate of 2 frames per second, with 200 ms exposure time.

The fluorescence time-trace of individual DNA-SWCNT nanosensors in response to thiocholine was extracted using ImageJ[68].

Results and Discussion

DNA-SWCNT Library Response to AChE and Acetylthiocholine

We chose a screening assay approach, based on previous successful demonstrations of SWCNT-sensors discovery, to find an optimal cholinesterase SWCNT-based sensor. In this approach, a library of DNA-SWCNTs are exposed to various analytes, establishing the specificity and sensitivity of these suspensions towards the selected analytes[40,45,50,69,70]. To this end, we measured the fluorescence response of a library of DNA-SWCNTs, including $(GT)_{15}$-, $(T)_{30}$-, $(TAT)_4$-, $(GTTT)_7$-, and $(GC)_{30}$-SWCNT, to either AChE, its substrate acetylthiocholine (ATC), or their combination (Figure 12). The rational was to identify a DNA-SWCNT suspension that would selectively respond to the byproducts of the hydrolytic reaction between AChE and ATC, but would be inactive to each of the initial reactants.

$(GT)_{15}$-SWCNTs and $(T)_{30}$-SWCNTs exhibited significant fluorescence increase of ~50% and ~70%, respectively, of the (9,4) chirality, when exposed to the AChE+ATC combination, whereas the exposure to either AChE or ATC alone resulted in a negligible response. As such, they were chosen for further investigation. $(TAT)_4$-SWCNTs also exhibited a large response towards the AChE+ATC combination, however, it was not selective and responded significantly to AChE alone. $(GC)_{30}$-SWCNTs showed a selective but smaller response compared to

$(GT)_{15}$-SWCNTs and $(T)_{30}$-SWCNTs, and the response of $(GTTT)_7$-SWCNTs was relatively small and less selective (Figure S2).

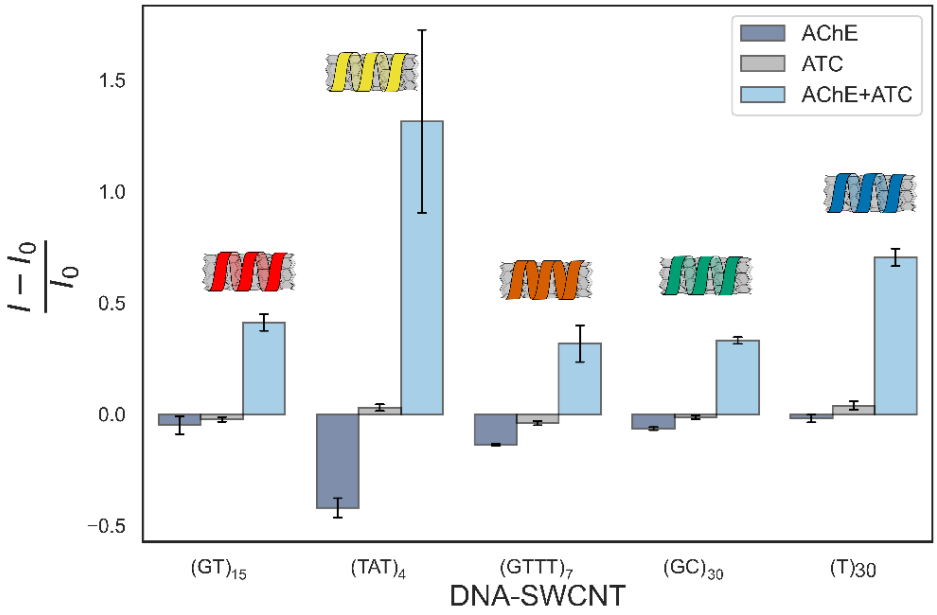

Figure 12: Normalized fluorescence response of different DNA-SWCNTs to either AChE, acetylthiocholine (ATC), or their combination (AChE + ATC). $(GT)_{15}$-SWCNT and $(T)_{30}$-SWCNT displayed a selective response towards the AChE+ATC combination. I_0 and I are the initial and final fluorescence intensities, respectively. All error bars represent the standard deviation of experimental replicates ($n = 3$).

Elucidating the Sensing Mechanism through the Response to Relevant Small Molecules

We exposed the sensors to varying concentrations of relevant small molecules to elucidate the exact chemical characteristics responsible for the fluorescence response of the DNA-SWCNTs during AChE enzymatic activity (Figure S3). We measured the fluorescence response towards, acetylthiocholine, the hydrolysis substrate, acetic acid and thiocholine, the hydrolysis products, as well as cysteine and choline to further probe the chemical functional groups responsible for the fluorescence response of the DNA-SWCNT sensors. We also measured the response toward an AChE inhibitor, neostigmine, at relevant concentrations.

We found a concentration-dependent significant fluorescence intensity response for both $(GT)_{15}$-SWCNTs and $(T)_{30}$-SWCNTs to thiocholine. The rest of the tested molecules induced small to negligible responses. Previously developed AChE-sensors relied on targeting or recognizing the thiol group present in thiocholine[10,17,21], which may partly contribute to the fluorescence response in our case. To test this option, we monitored the response to cysteine, a thiol-containing small molecule, and found a ~25% fluorescence increase at the relevant thiol concentrations for $(T)_{30}$-SWCNTs and a ~35% fluorescence increase for $(GT)_{15}$-SWCNTs (Figure S3). These values are smaller than expected if the mechanism was a simple recognition of thiols, in which case the response to thiols would be similar to the response to thiocholine. Therefore, the sensing cannot be explained by recognition of the thiol group, but rather a more complex mechanism governs the interaction and the resulting fluorescence response, possibly secondary coating structure modulation[28,71]. The fluorescence response of $(GT)_{15}$-SWCNTs and $(T)_{30}$-SWCNTs to acetylthiocholine at large concentrations might be attributed to spontaneous hydrolysis of acetylthiocholine to thiocholine during the assay.

Sensor Calibration with Different Concentrations of AChE and BChE

As the DNA-SWCNT sensors detect thiocholine, the sensors are also suitable for detecting ChE activity. Thus, we monitored the fluorescence response of the DNA-SWCNT sensors to different concentrations of both AChE and BChE between 10^{-4} and 10^{2} U L^{-1} well within the relevant window for characterizing enzymatic activity and inhibition in the body[72].

The concentration-dependent normalized fluorescence response was fitted by a four parameter logistic regression with a zero baseline, resulting in a three-parameter fit[50,51,73], $\frac{I-I_0}{I_0} = \beta \frac{x^n}{x^n+k^n}$, where I_0 and I are the initial and final fluorescence intensity, respectively, x is the cholinesterase activity units concentration, β is a proportion constant corresponding to the normalized fluorescence response at saturation, n is a cooperativity factor, and k is the inflection point (Figure 13). We have chosen a fit function that saturates as ATC is expected to be depleted in these assay conditions for activity units larger than 1 U L^{-1}, optimizing the response curve for physiological measurements. As such, the sigmoidal plots match the assay conditions and the amount of thiocholine present in the solution. Nevertheless, the assay conditions can be changed to fit the dynamic range of different ChE activity units. The fit parameters are summarized in the appendix (Table S1).

The k values obtained are in the range of 10^{-2}-10^{-1} U L^{-1}, and the response at saturation values, β, are in the range of 50-60%. Taking the experimental error into account, this fluorescence increase at saturation, resulting from the hydrolysis of 100 μM acetylthiocholine to thiocholine in the assay solution, is found to be in good agreement with the ~60-70% fluorescence increase seen when directly spiking the DNA-SWCNT sensor solutions with 100 μM thiocholine (Figure S3). The limit of detection was found to be in the 10^{-2} U L^{-1} range, mainly limited by the experimental error (Table S1), with values of 0.38 and 0.06 U L^{-1} for $(GT)_{15}$-SWCNTs for AChE

and BChE respectively, as well as values of 0.02 and 0.003 U L^{-1} for $(T)_{30}$-SWCNTs for AChE and BChE respectively. The time-dependent response for 1 U L^{-1} cholinesterase activity in both DNA-SWCNT sensors is shown in Figure 14. The fluorescence response to cholinesterase activity equilibrates after approximately one hour, showing an intensity increase for all measured DNA-SWCNT chiralities, most pronounced for the (9,4) chirality.

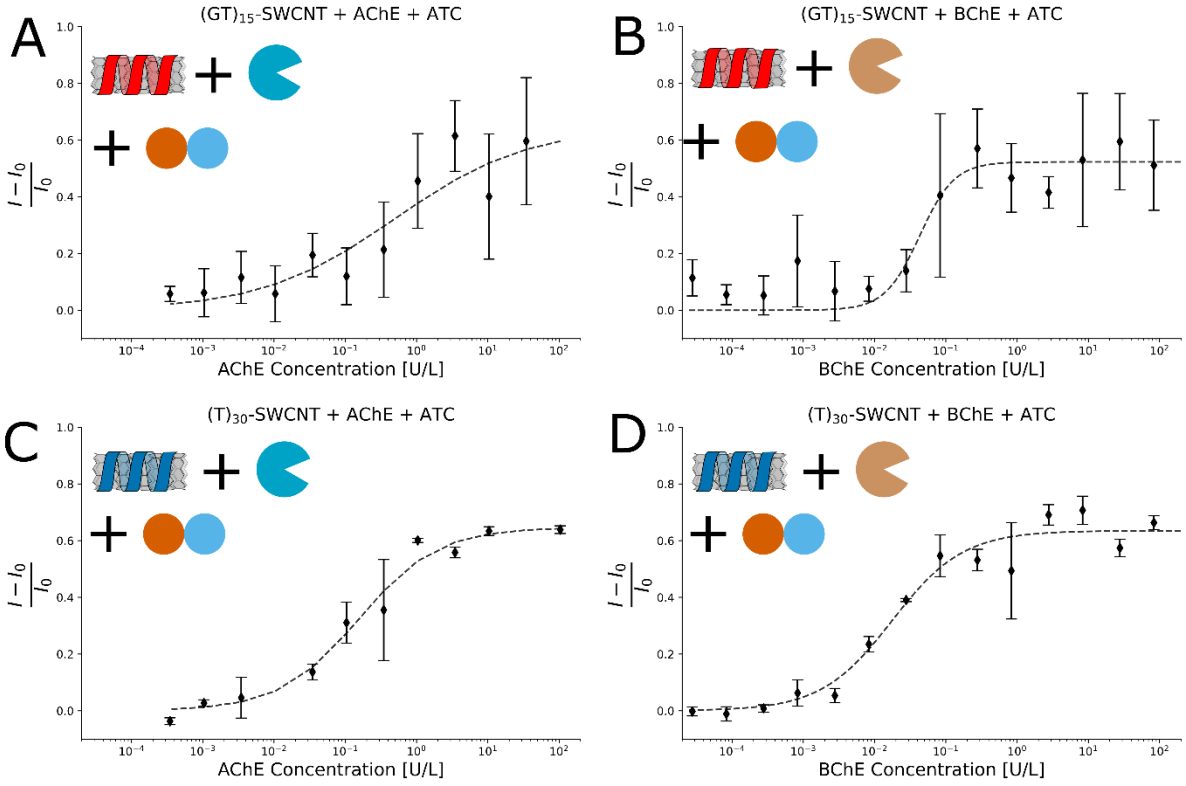

Figure 13: Fluorescence response of $(GT)_{15}$-SWCNT and $(T)_{30}$-SWCNT to different concentrations of AChE or BChE. (A) $(GT)_{15}$-SWCNTs and AChE, (B) $(GT)_{15}$-SWCNTs and BChE, (C) $(T)_{30}$-SWCNTs and AChE, (D) $(T)_{30}$-SWCNTs and BChE. All error bars represent the standard deviation of experimental replicates ($n = 3$). Four parameter logistic regression functions were fitted to the results (dashed lines), and their parameters can be found in the SI. The inflection points are in the range of 10^{-2} to 10^{-1} U L^{-1}.

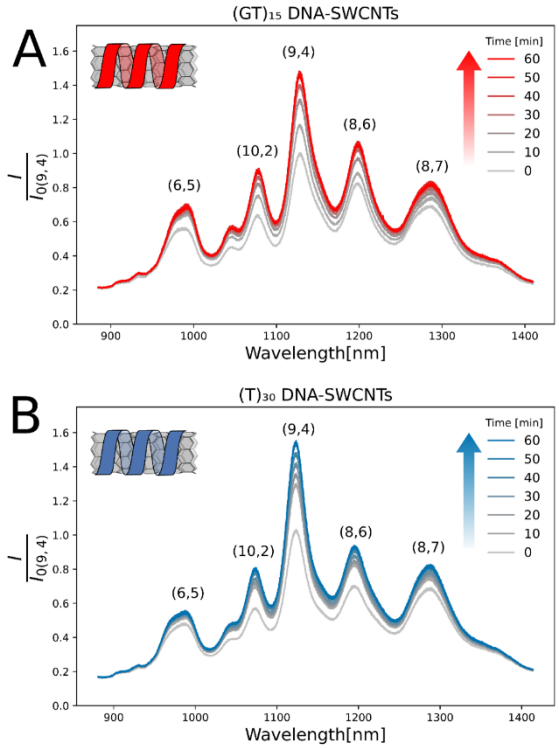

Figure 14: Time-dependent response of $(GT)_{15}$-SWCNTs (A) and $(T)_{30}$-SWCNTs (B) to 1 U L^{-1} AChE activity. The fluorescence response plateaus after about one hour (Figure S4).

Detecting Cholinesterase Inhibition

Neostigmine is an AChE inhibitor used for the treatment of myasthenia gravis[8]. Neostigmine blocks the activity of cholinesterase enzymes, thus, it prevents the hydrolysis of acetylthiocholine to thiocholine (Figure 15, top). Since our DNA-SWCNT sensors respond to the product of the cholinesterase hydrolysis, they can also be used to infer the enzymes are inhibited. We exposed BChE to an excess amount of neostigmine in order to block ChE activity, and then added the substrate acetylthiocholine. The fluorescence intensity response was recorded after one hour, and compared to the uninhibited BChE (Figure 15, bottom). We found a significant difference in the fluorescence response between the inhibited and uninhibited cholinesterase conditions, where the fluorescence intensity in the uninhibited case was more than three times larger than the inhibited. This demonstration paves the way for the detection of cholinesterase inhibition, which is important for a wide range of applications, from screening drug candidates[2] to detecting pesticides[74] and nerve agents[75,76].

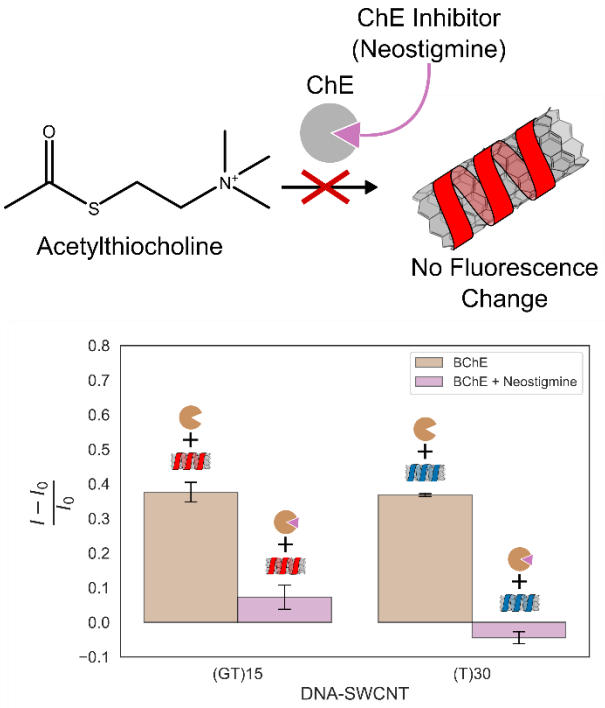

Figure 15: ChE inhibition by neostigmine illustration (top). Normalized fluorescence response of $(GT)_{15}$-SWCNTs and $(T)_{30}$-SWCNTs to inhibited and free BChE (bottom). A minimal fluorescence change is observed when a ChE inhibitor is present, compared to the significant response in the presence of the free ChE (P-value < 0.001 for both sensors). All error bars represent the standard deviation of experimental replicates ($n = 3$).

Detecting Serum Cholinesterase Activity

To demonstrate the applicability of the sensors to real-world samples, we measured cholinesterase activity in diluted fetal bovine serum. Serum samples were diluted 1:30, 1:90, and 1:300 in PBS, and their cholinesterase activity was measured separately by the Ellman method. $(GT)_{15}$-SWCNTs were incubated at 1 mg L^{-1} in diluted serum solution for two hours, after which 450 µM acetylthiocholine was added and the fluorescence intensity change was monitored for 12 minutes (Figure 16A). Each fluorescence intensity profile was fitted to an exponential function (Table S2). The slopes of the initial fluorescence intensity increase rate correlate well with the rate of production of the product of ChE activity measured by the Ellman assay (Figure 16B).

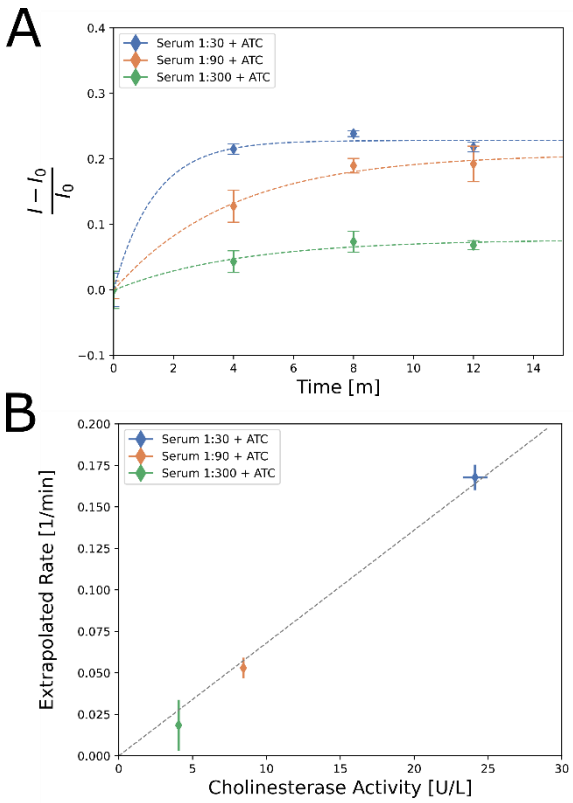

Figure 16. (A) Fluorescence intensity change of $(GT)_{15}$-SWCNTs to various serum dilutions upon the addition of 450 μM acetylthiocholine. Error bars represent the standard deviation of experimental replicates ($n = 3$). (B) The extrapolated rate constant from the slope at $t = 0$ of the exponential fit in (A) plotted as a function of the cholinesterase activity rate measured in serum by the Ellman method. A line was added as a guide to the eye. Error bars represent the 95% confidence intervals of the fit function ($n = 3$).

Spatiotemporal Nanosensor Fluorescence Imaging

In order to demonstrate the fluorescence response at the level of individual DNA-SWCNT sensors, we imaged surface-adsorbed $(GT)_{15}$-SWCNTs on a coverslip using HiLo microscopy[67] and monitored the fluorescence response upon the addition of 450 μM of thiocholine. We resolved individual nanotubes and observed an increase in fluorescence intensity of 150-180% upon thiocholine addition (Figure S6, Supporting video 1). Averaging the fluorescence intensity over the entire field of view (FOV) in response to the addition of thiocholine, we observed a 70% increase compared to the initial fluorescence intensity The higher response for individual SWCNT sensors, compared to the full FOV, is expected, since in the latter case, the areas without SWCNTs are taken into account in the calculation, masking the signal of the individual SWCNTs. This experiment demonstrates the potential for spatiotemporally resolving ChE activity in the near-infrared optical range using the DNA-SWCNT sensor platform.

Enzyme Activity Imaging

We then proceeded to measure the enzyme activity directly. SWCNTs in 450 µM acetylthiocholine were spiked with 5 µL of different BChE concentrations, and the fluorescence response was monitored (Figure 17, Supporting video 2). Analyzing the entire FOV, there is a clear fluorescence intensity increase in all samples, for which the kinetics depends on enzyme concentration. The fluorescence intensity increases by up to 70%, in agreement with the data presented in Figure S3 and Figure S6.

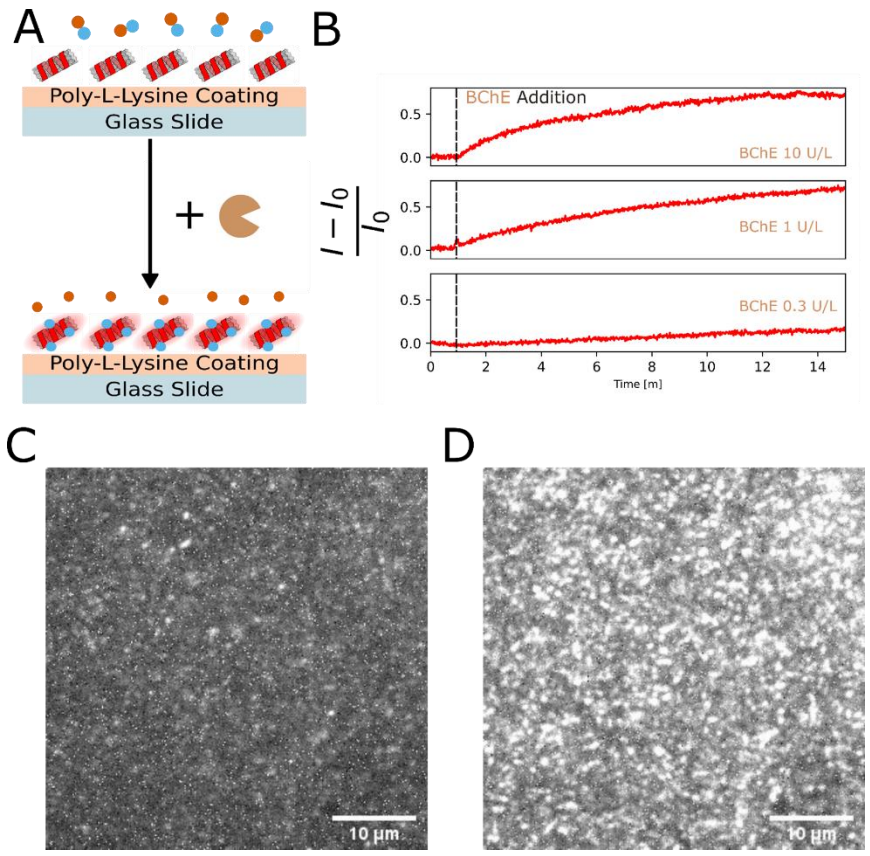

Figure 17: (A) Schematic diagram of the enzyme activity imaging experiment. (B) Full field of view fluorescence intensity time-traces showing the response to various cholinesterase concentrations added to SWCNTs with 450 µM acetylthiocholine. Images of $(GT)_{15}$-SWCNTs before (C) and after (D) the addition of butyrylcholinesterase. Images were extracted from a movie taken with a 100 × objective. Scale bars represent 10 µm.

Conclusion

We demonstrated two near-IR fluorescent single-walled carbon nanotube sensors for the measurement of cholinesterase activity and inhibition by screening five different DNA-SWCNTs candidates, and identifying two promising sensors, $(GT)_{15}$-SWCNTs and $(T)_{30}$-SWCNTs. These sensors showed a large and selective response towards thiocholine, the ChE hydrolysis product of acetylthiocholine, and almost no response to the substrate acetylthiocholine, the byproduct acetic acid, nor to the ChE inhibitor. The sensors fluorescence response was concentration-dependent, yielding LOD values in the range of 10^{-3}-10^{-1} U L^{-1}, well within the relevant concentration range for physiological measurements, and was demonstrated in serum samples. We demonstrated the sensors ability to infer the presence of cholinesterase inhibitors, manifested in a diminishing response compared to the free enzyme, by a factor of more than 3. Lastly, we imaged immobilized DNA-SWCNTs and observed an immediate fluorescence intensity increase in response to thiocholine and ChE activity at the level of individual nanosensors.

In summary, our DNA-SWCNT sensors for ChE activity and inhibition can be used in numerous settings where a rapid, *in situ,* reading of ChE activity is required, such as for sensing pesticide residues or for surgical guidance based on cancer-associated cholinesterase activity difference. Our work enables numerous applications using the option for spatiotemporal information of ChE activity and inhibition with our sensor platform and optical signal transduction in the biological transparency window.

References

(1) Dvir, H.; Silman, I.; Harel, M.; Rosenberry, T. L.; Sussman, J. L. Acetylcholinesterase: From 3D Structure to Function. *Chem. Biol. Interact.* **2010**, *187* (1–3), 10–22. https://doi.org/10.1016/j.cbi.2010.01.042.

(2) Musial, A.; Bajda, M.; Malawska, B. Recent Developments in Cholinesterases Inhibitors for Alzheimers Disease Treatment. *Curr. Med. Chem.* **2007**, *14* (25), 2654–2679. https://doi.org/10.2174/092986707782023217.

(3) Costanzi, S.; Machado, J. H.; Mitchell, M. Nerve Agents: What They Are, How They Work, How to Counter Them. *ACS Chem. Neurosci.* **2018**, *9* (5), 873–885. https://doi.org/10.1021/acschemneuro.8b00148.

(4) Suarez-Lopez, J. R.; Hood, N.; Suárez-Torres, J.; Gahagan, S.; Gunnar, M. R.; López-Paredes, D. Associations of Acetylcholinesterase Activity with Depression and Anxiety Symptoms among Adolescents Growing up near Pesticide Spray Sites. *Int. J. Hyg. Environ. Health* **2019**, *222* (7), 981–990. https://doi.org/10.1016/J.IJHEH.2019.06.001.

(5) Chatonnet, A.; Lockridge, O. Comparison of Butyrylcholinesterase and Acetylcholinesterase. *Biochem. J.* **1989**, *260* (3), 625–634. https://doi.org/10.1042/bj2600625.

(6) Harrington, C. T.; Hafid, N. Al; Waters, K. A. Butyrylcholinesterase Is a Potential Biomarker for Sudden Infant Death Syndrome. *EBioMedicine* **2022**, *80*, 104041. https://doi.org/10.1016/j.ebiom.2022.104041.

(7) Darvesh, S.; Hopkins, D. A.; Geula, C. Neurobiology of Butyrylcholinesterase. *Nat. Rev. Neurosci.* **2003**, *4* (2), 131–138. https://doi.org/10.1038/nrn1035.

(8) Quinn, D. M. Acetylcholinesterase: Enzyme Structure, Reaction Dynamics, and Virtual Transition States. *Chem. Rev.* **1987**, *87* (5), 955–979. https://doi.org/10.1021/cr00081a005.

(9) Marrs, T. T.; Maynard, R. L.; Sidell, F. *Chemical Warfare Agents: Toxicology and Treatment*; 2007.

(10) Ellman, G. L.; Courtney, K. D.; Andres, V.; Featherstone, R. M. A New and Rapid Colorimetric Determination of Acetylcholinesterase Activity. *Biochem. Pharmacol.* **1961**, *7* (2). https://doi.org/10.1016/0006-2952(61)90145-9.

(11) Wang, X.; Yang, Y.; Yin, Y.; Zeng, N.; Dong, Y.; Liu, J.; Wang, L.; Yang, Z.; Yang, C. High-Throughput Aptamer Microarrays for Fluorescent Detection of Multiple Organophosphorus Pesticides in Food. *Anal. Chem.* **2022**, *94* (7), 3173–3179. https://doi.org/10.1021/ACS.ANALCHEM.1C04650/ASSET/IMAGES/LARGE/AC1C04650_0003.JPEG.

(12) Ma, Y.; Gao, W.; Ma, S.; Liu, Y.; Lin, W. Observation of the Elevation of Cholinesterase Activity in Brain Glioma by a Near-Infrared Emission Chemsensor. *Anal. Chem.* **2020**, *92* (19), 13405–13410. https://doi.org/10.1021/ACS.ANALCHEM.0C02770.

(13) Ma, J.; Si, T.; Yan, C.; Li, Y.; Li, Q.; Lu, X.; Guo, Y. Near-Infrared Fluorescence Probe for Evaluating Acetylcholinesterase Activity in PC12 Cells and In Situ Tracing AChE Distribution in Zebrafish. *ACS Sensors* **2019**, *5* (1), 83–92. https://doi.org/10.1021/ACSSENSORS.9B01717.

(14) Chao, S.; Krejci, E.; Bernard, V.; Leroy, J.; Jean, L.; Renard, P. Y. A Selective and Sensitive Near-Infrared Fluorescent Probe for

Acetylcholinesterase Imaging. *Chem. Commun.* **2016**, *52* (77), 11599–11602. https://doi.org/10.1039/c6cc05936h.

(15) Zhao, X.; Zhang, L.; Yan, X.; Zhang, L.; Lu, Y.; Pan, J.; Zhang, M.; Wang, C.; Suo, H.; Jia, X.; Liu, X.; Lu, G. A Near-Infrared Light Triggered Fluormetric Biosensor for Sensitive Detection of Acetylcholinesterase Activity Based on NaErF4: 0.5 % Ho3+@NaYF4 Upconversion Nano-Probe. *Talanta* **2021**, *235*, 122784. https://doi.org/10.1016/J.TALANTA.2021.122784.

(16) Korram, J.; Dewangan, L.; Karbhal, I.; Nagwanshi, R.; Vaishanav, S. K.; Ghosh, K. K.; Satnami, M. L. CdTe QD-Based Inhibition and Reactivation Assay of Acetylcholinesterase for the Detection of Organophosphorus Pesticides. *RSC Adv.* **2020**, *10* (41), 24190–24202. https://doi.org/10.1039/d0ra03055d.

(17) Zhang, Y.; Cai, Y.; Qi, Z.; Lu, L.; Qian, Y. DNA-Templated Silver Nanoclusters for Fluorescence Turn-on Assay of Acetylcholinesterase Activity. *Anal. Chem.* **2013**, *85* (17), 8455–8461. https://doi.org/10.1021/ac401966d.

(18) Peng, L.; Zhang, G.; Zhang, D.; Xiang, J.; Zhao, R.; Wang, Y.; Zhu, D. A Fluorescence “Turn-On” Ensemble for Acetylcholinesterase Activity Assay and Inhibitor Screening. *Org. Lett.* **2009**, *11* (17), 4014–4017. https://doi.org/10.1021/OL9016723.

(19) Cui, K.; Chen, Z.; Wang, Z.; Zhang, G.; Zhang, D. A Naked-Eye Visible and Fluorescence “Turn-on” Probe for Acetyl-Cholinesterase Assay and Thiols as Well as Imaging of Living Cells. *Analyst* **2011**, *136* (1), 191–195. https://doi.org/10.1039/c0an00456a.

(20) Xu, X.; Cen, Y.; Xu, G.; Wei, F.; Shi, M.; Hu, Q. A Ratiometric Fluorescence Probe Based on Carbon Dots for Discriminative and Highly Sensitive Detection of Acetylcholinesterase and Butyrylcholinesterase in Human Whole Blood. *Biosens. Bioelectron.* **2019**, *131*, 232–236. https://doi.org/10.1016/J.BIOS.2019.02.031.

(21) Wang, M.; Liu, L.; Xie, X.; Zhou, X.; Lin, Z.; Su, X. Single-Atom Iron Containing Nanozyme with Peroxidase-like Activity and Copper Nanoclusters Based Ratio Fluorescent Strategy for Acetylcholinesterase Activity Sensing. *Sensors Actuators B Chem.* **2020**, *313*, 128023. https://doi.org/10.1016/J.SNB.2020.128023.

(22) Worek, F.; Mast, U.; Kiderlen, D.; Diepold, C.; Eyer, P. Improved Determination of Acetylcholinesterase Activity in Human Whole Blood. *Clinica Chimica Acta*. 1999, pp 73–90. https://doi.org/10.1016/S0009-8981(99)00144-8.

(23) Worek, F.; Eyer, P.; Thiermann, H. Determination of Acetylcholinesterase Activity by the Ellman Assay: A Versatile Tool for in Vitro Research on Medical Countermeasures against Organophosphate Poisoning. *Drug Test. Anal.* **2012**, *4* (3–4), 282–291. https://doi.org/10.1002/dta.337.

(24) Ash, C.; Dubec, M.; Donne, K.; Bashford, T. Effect of Wavelength and Beam Width on Penetration in Light-Tissue Interaction Using Computational Methods. *Lasers Med. Sci.* **2017**, *32* (8), 1909–1918. https://doi.org/10.1007/s10103-017-2317-4.

(25) Billinton, N.; Knight, A. W. Seeing the Wood through the Trees: A Review of Techniques for Distinguishing Green Fluorescent Protein from Endogenous Autofluorescence. *Anal. Biochem.* **2001**, *291* (2), 175–197.

https://doi.org/10.1006/abio.2000.5006.

(26) Pansare, V. J.; Hejazi, S.; Faenza, W. J.; Prud'Homme, R. K. Review of Long-Wavelength Optical and NIR Imaging Materials: Contrast Agents, Fluorophores, and Multifunctional Nano Carriers. *Chem. Mater.* **2012**, *24* (5), 812–827. https://doi.org/10.1021/cm2028367.

(27) Kruss, S.; Hilmer, A. J.; Zhang, J.; Reuel, N. F.; Mu, B.; Strano, M. S. Carbon Nanotubes as Optical Biomedical Sensors. *Adv. Drug Deliv. Rev.* **2013**, *65* (15), 1933–1950. https://doi.org/10.1016/j.addr.2013.07.015.

(28) Ackermann, J.; Metternich, J. T.; Herbertz, S.; Kruss, S. Biosensing with Fluorescent Carbon Nanotubes. *Angew. Chemie - Int. Ed.* **2022**, *61* (18), e202112372. https://doi.org/10.1002/anie.202112372.

(29) De Los Santos, Z. A.; Lin, Z.; Zheng, M. Optical Detection of Stereoselective Interactions with DNA-Wrapped Single-Wall Carbon Nanotubes. *J. Am. Chem. Soc.* **2021**, *143* (49), 20628–20632. https://doi.org/10.1021/jacs.1c11372.

(30) Wang, F.; Dukovic, G.; Brus, L. E.; Heinz, T. F. The Optical Resonances in Carbon Nanotubes Arise from Excitons. *Science (80-.).* **2005**, *308* (5723), 838–841. https://doi.org/10.1126/science.1110265.

(31) O'Connell, M. J.; Bachilo, S. H.; Huffman, C. B.; Moore, V. C.; Strano, M. S.; Haroz, E. H.; Rialon, K. L.; Boul, P. J.; Noon, W. H.; Kittrell, C.; Ma, J.; Hauge, R. H.; Weisman, R. B.; Smalley, R. E. Band Gap Fluorescence from Individual Single-Walled Carbon Nanotubes. *Science (80-.).* **2002**, *297* (5581), 593–596. https://doi.org/10.1126/science.1072631.

(32) Bachilo, S. M.; Strano, M. S.; Kittrell, C.; Hauge, R. H.; Smalley, R. E.;

Weisman, R. B. Structure-Assigned Optical Spectra of Single-Walled Carbon Nanotubes. *Science (80-.).* **2002**, *298* (5602), 2361–2366. https://doi.org/10.1126/science.1078727.

(33) Lüer, L.; Hoseinkhani, S.; Polli, D.; Crochet, J.; Hertel, T.; Lanzani, G. Size and Mobility of Excitons in (6, 5) Carbonnanotubes. *Nat. Phys.* **2009**, *5* (1), 54–58. https://doi.org/10.1038/nphys1149.

(34) Siitonen, A. J.; Tsyboulski, D. A.; Bachilo, S. M.; Weisman, R. B. Surfactant-Dependent Exciton Mobility in Single-Walled Carbon Nanotubes Studied by Single-Molecule Reactions. *Nano Lett.* **2010**, *10* (5), 1595–1599. https://doi.org/10.1021/nl9039845.

(35) Manzoni, C.; Gambetta, A.; Menna, E.; Meneghetti, M.; Lanzani, G.; Cerullo, G. Intersubband Exciton Relaxation Dynamics in Single-Walled Carbon Nanotubes. *Phys. Rev. Lett.* **2005**, *94* (20), 2–5. https://doi.org/10.1103/PhysRevLett.94.207401.

(36) Iverson, N. M.; Barone, P. W.; Shandell, M.; Trudel, L. J.; Sen, S.; Sen, F.; Ivanov, V.; Atolia, E.; Farias, E.; McNicholas, T. P.; Reuel, N.; Parry, N. M. A.; Wogan, G. N.; Strano, M. S. In Vivo Biosensing via Tissue-Localizable near-Infrared-Fluorescent Single-Walled Carbon Nanotubes. *Nat. Nanotechnol.* **2013**, *8* (11), 873–880. https://doi.org/10.1038/nnano.2013.222.

(37) Wu, H.; Nißler, R.; Morris, V.; Herrmann, N.; Hu, P.; Jeon, S. J.; Kruss, S.; Giraldo, J. P. Monitoring Plant Health with Near-Infrared Fluorescent H2O2 Nanosensors. *Nano Lett.* **2020**, *20* (4), 2432–2442. https://doi.org/10.1021/acs.nanolett.9b05159.

(38) Wong, M. H.; Giraldo, J. P.; Kwak, S. Y.; Koman, V. B.; Sinclair, R.; Lew,

T. T. S.; Bisker, G.; Liu, P.; Strano, M. S. Nitroaromatic Detection and Infrared Communication from Wild-Type Plants Using Plant Nanobionics. *Nat. Mater.* **2017**, *16* (2), 264–272. https://doi.org/10.1038/nmat4771.

(39) Bisker, G. Optical Nanosensors in the Near-Infrared Spectral Window. In *2021 Conference on Lasers and Electro-Optics (CLEO)*; 2021; pp 1–2.

(40) Lee, M. A.; Wang, S.; Jin, X.; Bakh, N. A.; Nguyen, F. T.; Dong, J.; Silmore, K. S.; Gong, X.; Pham, C.; Jones, K. K.; Muthupalani, S.; Bisker, G.; Son, M.; Strano, M. S. Implantable Nanosensors for Human Steroid Hormone Sensing In Vivo Using a Self-Templating Corona Phase Molecular Recognition. *Adv. Healthc. Mater.* **2020**, *2000429* (21), 1–13. https://doi.org/10.1002/adhm.202000429.

(41) Beyene, A. G.; Delevich, K.; Del Bonis-O'Donnell, J. T.; Piekarski, D. J.; Lin, W. C.; Wren Thomas, A.; Yang, S. J.; Kosillo, P.; Yang, D.; Prounis, G. S.; Wilbrecht, L.; Landry, M. P. Imaging Striatal Dopamine Release Using a Nongenetically Encoded near Infrared Fluorescent Catecholamine Nanosensor. *Sci. Adv.* **2019**, *5* (7), eaaw3108. https://doi.org/10.1126/sciadv.aaw3108.

(42) Bakh, N. A.; Gong, X.; Lee, M. A.; Jin, X.; Koman, V. B.; Park, M.; Nguyen, F. T.; Strano, M. S. Transcutaneous Measurement of Essential Vitamins Using Near-Infrared Fluorescent Single-Walled Carbon Nanotube Sensors. *Small* **2021**, *17* (31), 2100540. https://doi.org/10.1002/smll.202100540.

(43) Paviolo, C.; Cognet, L. Near-Infrared Nanoscopy with Carbon-Based Nanoparticles for the Exploration of the Brain Extracellular Space. *Neurobiol. Dis.* **2021**, *153*, 105328. https://doi.org/10.1016/j.nbd.2021.105328.

(44) Zhang, J.; Landry, M. P.; Barone, P. W.; Kim, J. H.; Lin, S.; Ulissi, Z. W.; Lin, D.; Mu, B.; Boghossian, A. A.; Hilmer, A. J.; Rwei, A.; Hinckley, A. C.; Kruss, S.; Shandell, M. A.; Nair, N.; Blake, S.; Şen, F.; Şen, S.; Croy, R. G.; Li, D.; Yum, K.; Ahn, J. H.; Jin, H.; Heller, D. A.; Essigmann, J. M.; Blankschtein, D.; Strano, M. S. Molecular Recognition Using Corona Phase Complexes Made of Synthetic Polymers Adsorbed on Carbon Nanotubes. *Nat. Nanotechnol.* **2013**, *8* (12), 959–968. https://doi.org/10.1038/nnano.2013.236.

(45) Kruss, S.; Landry, M. P.; Vander Ende, E.; Lima, B. M. A.; Reuel, N. F.; Zhang, J.; Nelson, J.; Mu, B.; Hilmer, A.; Strano, M. Neurotransmitter Detection Using Corona Phase Molecular Recognition on Fluorescent Single-Walled Carbon Nanotube Sensors. *J. Am. Chem. Soc.* **2014**, *136* (2), 713–724. https://doi.org/10.1021/ja410433b.

(46) Bulumulla, C.; Krasley, A. T.; Walpita, D.; Beyene, A. G. Visualizing Synaptic Dopamine Efflux with a 2D Nanofilm. *bioRxiv* **2022**, 2022.01.19.476937. https://doi.org/10.1101/2022.01.19.476937.

(47) Yang, S. J.; Del Bonis-O'Donnell, J. T.; Beyene, A. G.; Landry, M. P. Near-Infrared Catecholamine Nanosensors for High Spatiotemporal Dopamine Imaging. *Nat. Protoc. 2021 166* **2021**, *16* (6), 3026–3048. https://doi.org/10.1038/s41596-021-00530-4.

(48) Bisker, G.; Dong, J.; Park, H. D.; Iverson, N. M.; Ahn, J.; Nelson, J. T.; Landry, M. P.; Kruss, S.; Strano, M. S. Protein-Targeted Corona Phase Molecular Recognition. *Nat. Commun.* **2016**, *7*. https://doi.org/10.1038/ncomms10241.

(49) Wulf, V.; Slor, G.; Rathee, P.; Amir, R. J.; Bisker, G. Dendron–Polymer

Hybrids as Tailorable Responsive Coronae of Single-Walled Carbon Nanotubes. *ACS Nano* **2021**, acsnano.1c09125. https://doi.org/10.1021/acsnano.1c09125.

(50) Bisker, G.; Bakh, N. A.; Lee, M. A.; Ahn, J.; Park, M.; O'Connell, E. B.; Iverson, N. M.; Strano, M. S.; Connell, E. B. O.; Iverson, N. M.; Strano, M. S.; O'Connell, E. B.; Iverson, N. M.; Strano, M. S. Insulin Detection Using a Corona Phase Molecular Recognition Site on Single-Walled Carbon Nanotubes. *ACS Sensors* **2018**, *3* (2), 367–377. https://doi.org/10.1021/acssensors.7b00788.

(51) Ehrlich, R.; Hendler-Neumark, A.; Wulf, V.; Amir, D.; Bisker, G. Optical Nanosensors for Real-Time Feedback on Insulin Secretion by β-Cells. *Small* **2021**, *17* (30), 2101660. https://doi.org/10.1002/SMLL.202101660.

(52) Hendler-Neumark, A.; Bisker, G. Fluorescent Single-Walled Carbon Nanotubes for Protein Detection. *Sensors (Switzerland)*. MDPI AG December 2, 2019, p 5403. https://doi.org/10.3390/s19245403.

(53) Cho, S.-Y.; Jin, X.; Gong, X.; Yang, S.; Cui, J.; Strano, M. S. Antibody-Free Rapid Detection of SARS-CoV-2 Proteins Using Corona Phase Molecular Recognition to Accelerate Development Time. *Anal. Chem.* **2021**, *93* (44), 14685–14693. https://doi.org/10.1021/ACS.ANALCHEM.1C02889.

(54) Nißler, R.; Müller, A. T.; Dohrman, F.; Kurth, L.; Li, H.; Cosio, E. G.; Flavel, B. S.; Giraldo, J. P.; Mithöfer, A.; Kruss, S. Detection and Imaging of the Plant Pathogen Response by Near-Infrared Fluorescent Polyphenol Sensors. *Angew. Chemie Int. Ed.* **2022**, *61* (2), e202108373. https://doi.org/10.1002/ANIE.202108373.

(55) Antman-Passig, M.; Wong, E.; Frost, G. R.; Cupo, C.; Shah, J.; Agustinus,

A.; Chen, Z.; Mancinelli, C.; Kamel, M.; Li, T.; Jonas, L. A.; Li, Y.-M.; Heller, D. A. Optical Nanosensor for Intracellular and Intracranial Detection of Amyloid-Beta. *ACS Nano* **2022**, *08*, acsnano.2c00054. https://doi.org/10.1021/ACSNANO.2C00054.

(56) Kim, M.; Chen, C.; Wang, P.; Mulvey, J. J.; Yang, Y.; Wun, C.; Antman-Passig, M.; Luo, H. Bin; Cho, S.; Long-Roche, K.; Ramanathan, L. V.; Jagota, A.; Zheng, M.; Wang, Y. H.; Heller, D. A. Detection of Ovarian Cancer via the Spectral Fingerprinting of Quantum-Defect-Modified Carbon Nanotubes in Serum by Machine Learning. *Nat. Biomed. Eng. 2022 63* **2022**, *6* (3), 267–275. https://doi.org/10.1038/s41551-022-00860-y.

(57) Langenbacher, R.; Budhathoki-Uprety, J.; Jena, P. V.; Roxbury, D.; Streit, J.; Zheng, M.; Heller, D. A. Single-Chirality Near-Infrared Carbon Nanotube Sub-Cellular Imaging and FRET Probes. *Nano Lett.* **2021**, *21* (15), 6441–6448. https://doi.org/10.1021/ACS.NANOLETT.1C01093/SUPPL_FILE/NL1C01093_SI_001.PDF.

(58) Hofferber, E.; Meier, J.; Herrera, N.; Stapleton, J.; Calkins, C.; Iverson, N. Detection of Single Walled Carbon Nanotube Based Sensors in a Large Mammal. *Nanomedicine Nanotechnology, Biol. Med.* **2022**, *40*, 102489. https://doi.org/10.1016/J.NANO.2021.102489.

(59) Nißler, R.; Bader, O.; Dohmen, M.; Walter, S. G.; Noll, C.; Selvaggio, G.; Groß, U.; Kruss, S. Remote near Infrared Identification of Pathogens with Multiplexed Nanosensors. *Nat. Commun.* **2020**, *11* (1), 1–12. https://doi.org/10.1038/s41467-020-19718-5.

(60) Shumeiko, V.; Zaken, Y.; Hidas, G.; Paltiel, Y.; Bisker, G.; Shoseyov, O.

Peptide-Encapsulated Single-Wall Carbon Nanotube-Based near-Infrared Optical Nose for Bacteria Detection and Classification. *IEEE Sens. J.* **2022**, 1. https://doi.org/10.1109/JSEN.2022.3152622.

(61) Shumeiko, V.; Malach, E.; Helman, Y.; Paltiel, Y.; Bisker, G.; Hayouka, Z.; Shoseyov, O. A Nanoscale Optical Biosensor Based on Peptide Encapsulated SWCNTs for Detection of Acetic Acid in the Gaseous Phase. *Sensors Actuators B Chem.* **2021**, *327*, 128832. https://doi.org/10.1016/j.snb.2020.128832.

(62) Shumeiko, V.; Paltiel, Y.; Bisker, G.; Hayouka, Z.; Shoseyov, O. A Nanoscale Paper-Based near-Infrared Optical Nose (NIRON). *Biosens. Bioelectron.* **2021**, *172*, 112763. https://doi.org/10.1016/j.bios.2020.112763.

(63) Yaari, Z.; Cheung, J. M.; Baker, H. A.; Frederiksen, R. S.; Jena, P. V.; Horoszko, C. P.; Jiao, F.; Scheuring, S.; Luo, M.; Heller, D. A. Nanoreporter of an Enzymatic Suicide Inactivation Pathway. *Nano Lett.* **2020**. https://doi.org/10.1021/acs.nanolett.0c01858.

(64) Shumeiko, V.; Paltiel, Y.; Bisker, G.; Hayouka, Z.; Shoseyov, O. A Paper-Based Near-Infrared Optical Biosensor for Quantitative Detection of Protease Activity Using Peptide-Encapsulated SWCNTs. *Sensors* **2020**, *20* (18), 5247. https://doi.org/10.3390/s20185247.

(65) Loewenthal, D.; Kamber, D.; Bisker, G. Monitoring the Activity and Inhibition of Cholinesterase Enzymes Using Single-Walled Carbon Nanotube Fluorescent Sensors. *Anal. Chem.* **2022**, 94 (41), 14223-14231 https://doi.org/10.1021/acs.analchem.2c02471.

(66) Hendler-Neumark, A.; Wulf, V.; Bisker, G. In Vivo Imaging of Fluorescent Single-Walled Carbon Nanotubes within C. Elegans Nematodes in the near-

Infrared Window. *Mater. Today Bio* **2021**, *12* (September), 100175. https://doi.org/10.1016/j.mtbio.2021.100175.

(67) Tokunaga, M.; Imamoto, N.; Sakata-Sogawa, K. Highly Inclined Thin Illumination Enables Clear Single-Molecule Imaging in Cells. *Nat. Methods 2008 52* **2008**, *5* (2), 159–161. https://doi.org/10.1038/nmeth1171.

(68) Rasband, W. S. ImageJ. U. S. National Institutes of Health: Bethesda, Maryland, USA.

(69) Amir, D.; Hendler-Neumark, A.; Wulf, V.; Ehrlich, R.; Bisker, G. Oncometabolite Fingerprinting Using Fluorescent Single-Walled Carbon Nanotubes. *Adv. Mater. Interfaces* **2022**, *9* (4). https://doi.org/10.1002/admi.202101591.

(70) Salem, D. P.; Landry, M. P.; Bisker, G.; Ahn, J.; Kruss, S.; Strano, M. S. Chirality Dependent Corona Phase Molecular Recognition of DNA-Wrapped Carbon Nanotubes. *Carbon N. Y.* **2016**, *97*. https://doi.org/10.1016/j.carbon.2015.08.075.

(71) Heller, D. A.; Pratt, G. W.; Zhang, J.; Nair, N.; Hansborough, A. J.; Boghossian, A. A.; Reuel, N. F.; Barone, P. W.; Strano, M. S. Peptide Secondary Structure Modulates Single-Walled Carbon Nanotube Fluorescence as a Chaperone Sensor for Nitroaromatics. *Proc. Natl. Acad. Sci. U. S. A.* **2011**, *108* (21), 8544–8549. https://doi.org/10.1073/PNAS.1005512108/SUPPL_FILE/PNAS.1005512108_SI.PDF.

(72) Lopez-Carillo, L.; Lopez-Crevantes, M. Effect of Exposure to Organophosphate Pesticides on Serum c Hol i Nesterase Levels. *Arch. Environ. Health* **1993**, *48* (5), 359–363.

https://doi.org/10.1080/00039896.1993.9936726.

(73) Jeong, S.; Yang, D.; Beyene, A. G.; Del Bonis-O'Donnell, J. T.; Gest, A. M. M.; Navarro, N.; Sun, X.; Landry, M. P. High-Throughput Evolution of near-Infrared Serotonin Nanosensors. *Sci. Adv.* **2019**, *5* (12), 3771–3789. https://doi.org/10.1126/sciadv.aay3771.

(74) Pundir, C. S.; Chauhan, N. Acetylcholinesterase Inhibition-Based Biosensors for Pesticide Determination: A Review. *Anal. Biochem.* **2012**, *429* (1), 19–31. https://doi.org/10.1016/j.ab.2012.06.025.

(75) Zhang, W.; Guo, Z.; Chen, Y.; Cao, Y. Nanomaterial Based Biosensors for Detection of Biomarkers of Exposure to OP Pesticides and Nerve Agents: A Review. *Electroanalysis* **2017**, *29* (5), 1206–1213. https://doi.org/10.1002/elan.201600748.

(76) Chen, L.; Wu, D.; Yoon, J. Recent Advances in the Development of Chromophore-Based Chemosensors for Nerve Agents and Phosgene. *ACS Sensors* **2018**, *3* (1), 27–43. https://doi.org/10.1021/acssensors.7b00816.

Appendix

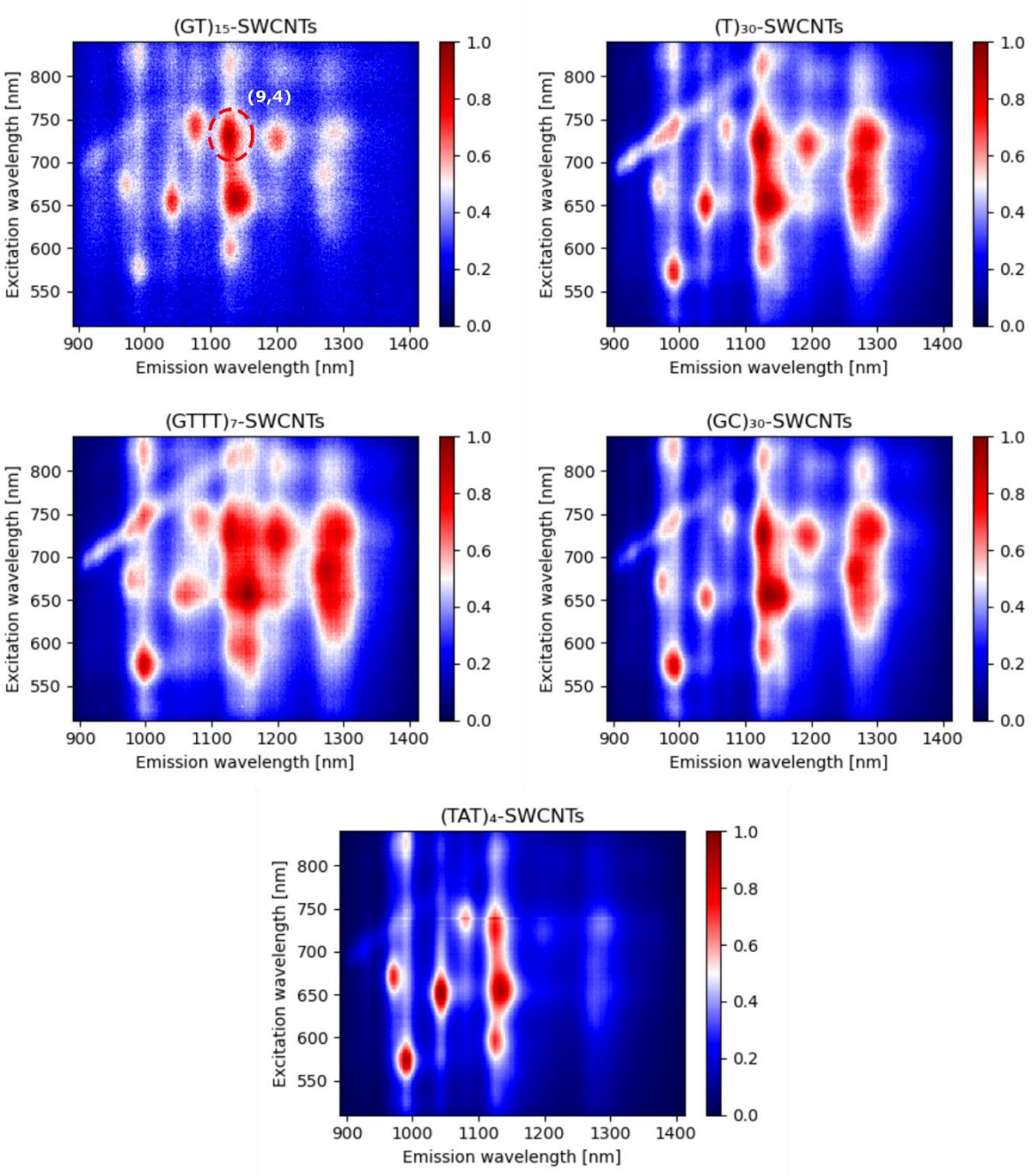

Figure S1. Excitation-emission fluorescence spectra of screened DNA-SWCNTs. The (9,4) chirality is highlighted for $(GT)_{15}$-SWCNTs.

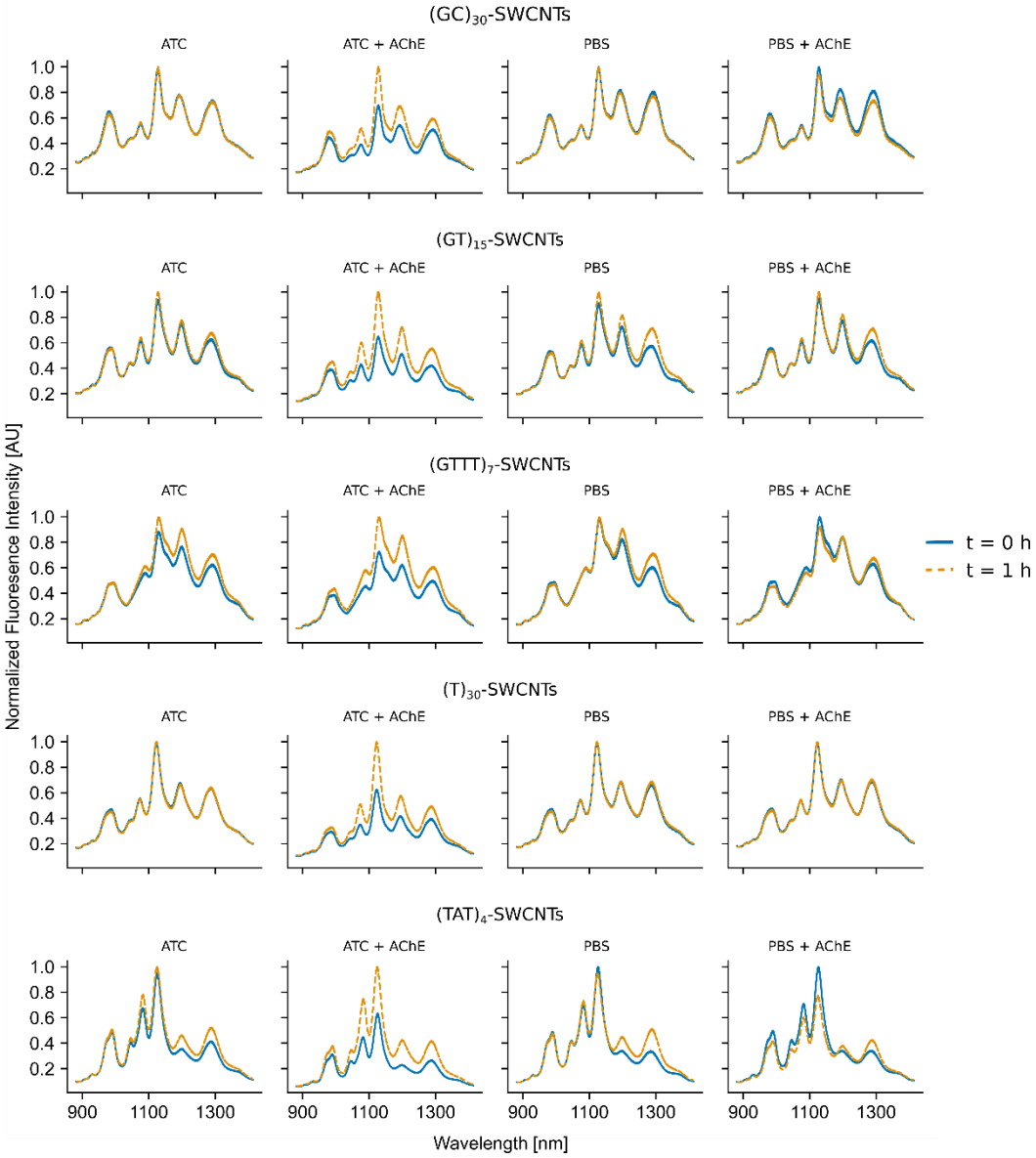

Figure S2. DNA-SWCNTs screening results. Each row shows a different sensor, and each column shows a different analyte addition (from left to right): acetylthiocholine (ATC), ATC followed by acetylcholinesterase (AChE), PBS, PBS followed by AChE. The blue lines are the fluorescence intensity at $t = 0$ upon the addition of the analyte, and the orange lines are the fluorescence intensity at $t = 1\ h$. Each spectrum contains the average data of three different experiments. The chosen sensors, $(GT)_{15}$-SWCNT and $(T)_{30}$-SWCNT, show no response to PBS, AChE alone, nor acetylthiocholine alone, but show a fluorescence intensity increase in response to AChE in the presence of acetylthiocholine.

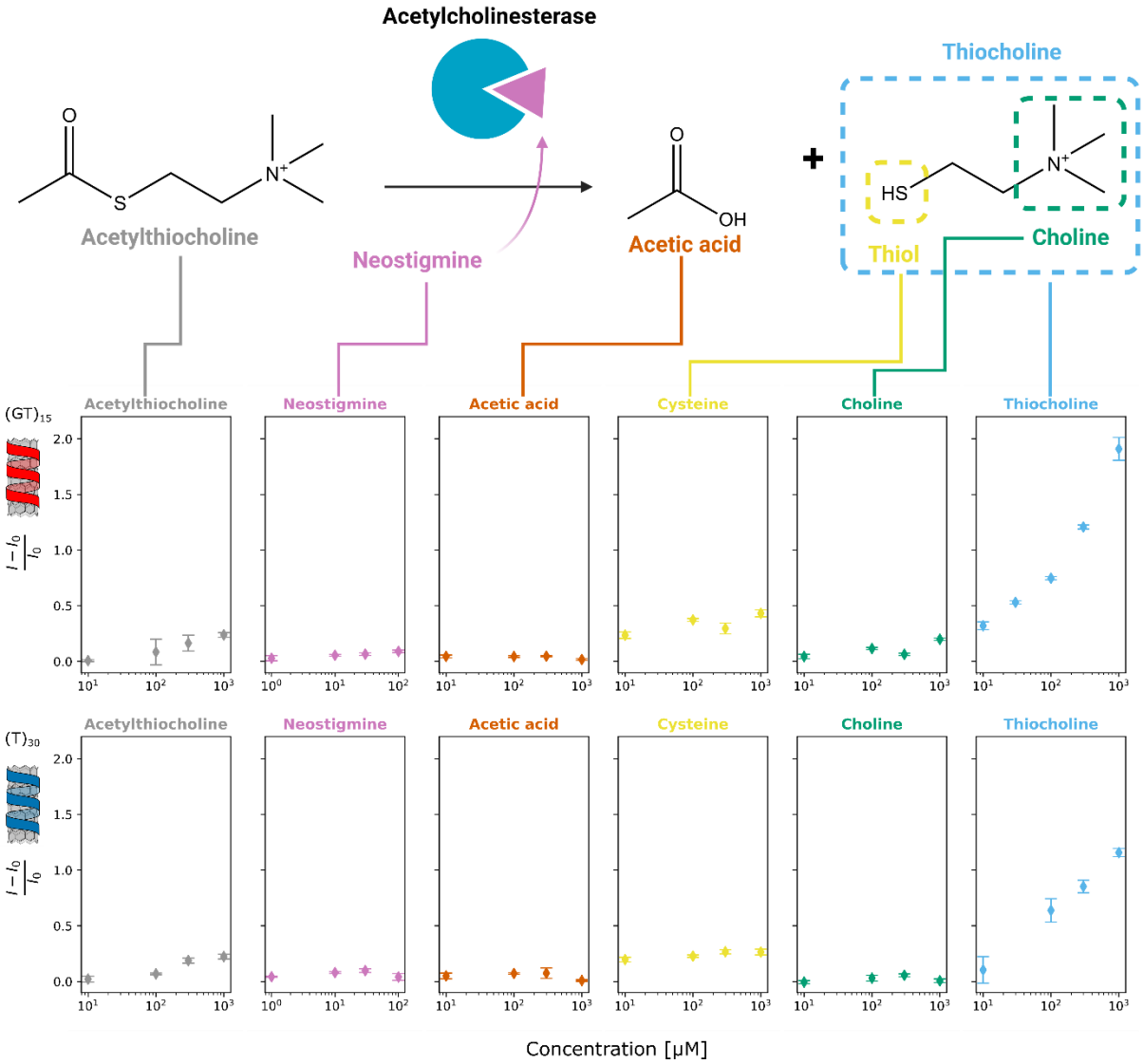

Figure S3. Relevant small molecules for the AChE-mediated hydrolysis of acetylthiocholine to acetic acid and thiocholine with\without the presence of an inhibitor (top row). Normalized fluorescence response of $(GT)_{15}$-SWCNTs (middle row) and $(T)_{30}$-SWCNTs (bottom row) nanosensors to small molecules. DNA-SWCNTs exhibit a large and concentration-dependent response for thiocholine, whereas other molecules induce a small to negligible response All error bars represent the standard deviation of experimental replicates ($n = 3$).

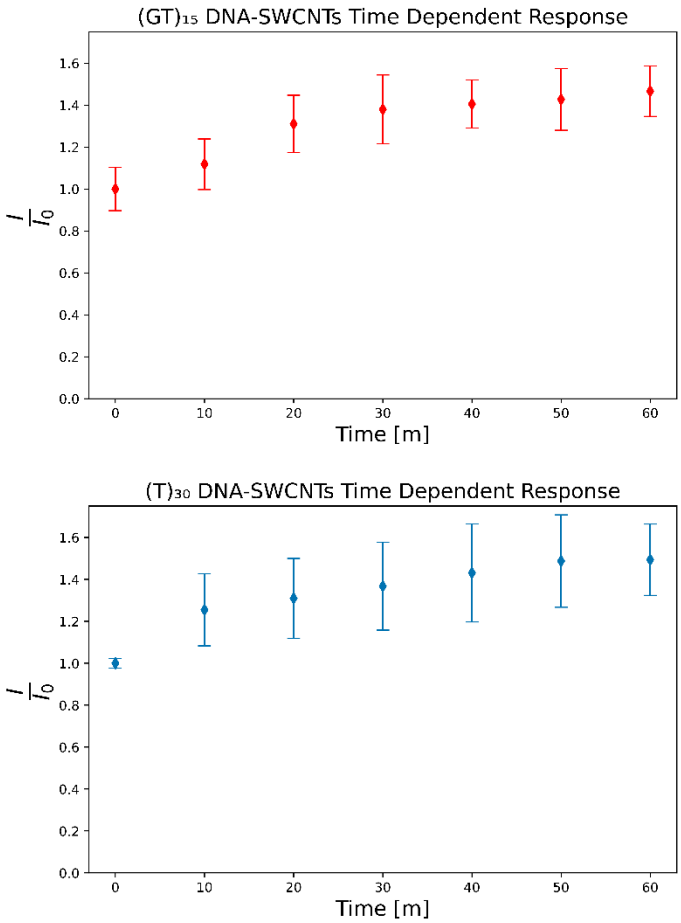

Figure S4. Time-dependent fluorescence intensity for the (9,4) chirality peak of $(GT)_{15}$-SWCNTs (top) and $(T)_{30}$-SWCNTs (bottom) in response to 1 U L^{-1} butyrylcholinesterase in the presence of acetylthiocholine. All error bars represent the standard deviation of experimental replicates ($n = 3$).

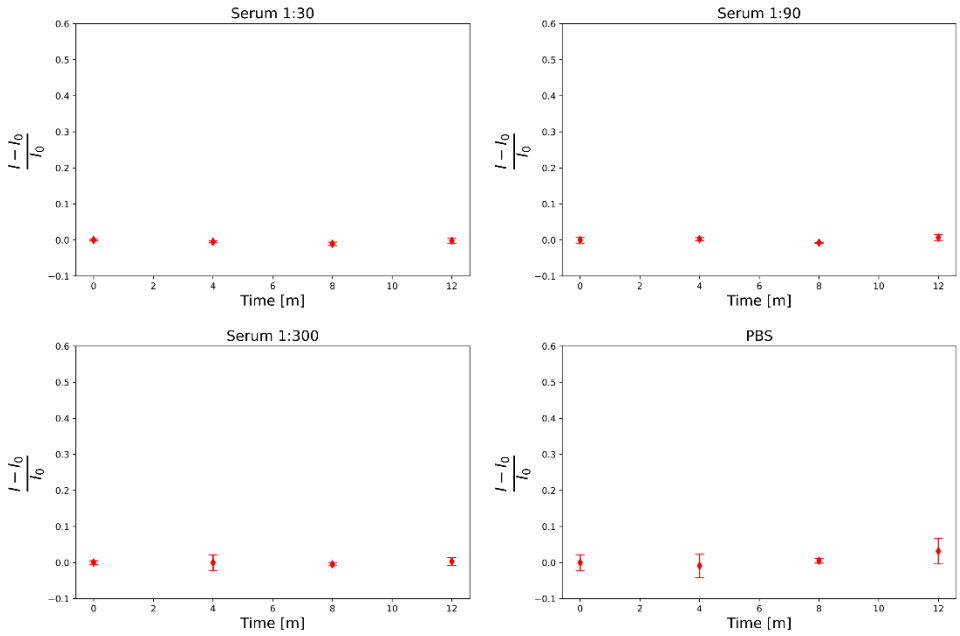

Figure S5. Time-dependent fluorescence intensity for the (9,4) chirality peak of $(GT)_{15}$-SWCNTs in various serum dilutions after two hours of incubation. There was little to no change in the fluorescence intensity of the SWCNTs during the serum cholinesterase activity assay.

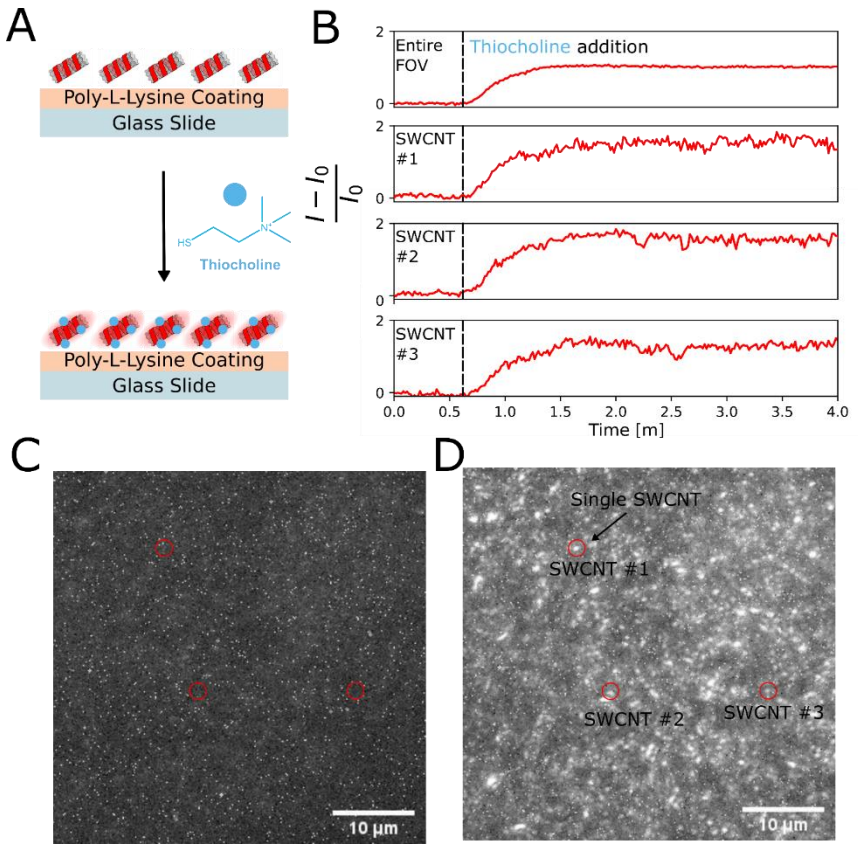

Figure S6. (A) Schematic diagram of the thiocholine imaging experiment. $(GT)_{15}$-SWCNTs were immobilized on a Poly-L-Lysine treated glass slide, to which thiocholine solution was added. (B) Fluorescence intensity response of the entire field of view (FOV) of single $(GT)_{15}$-SWCNTs (bottom graphs) during addition, showing a clear increase in fluorescence intensity upon thiocholine addition. Images of $(GT)_{15}$-SWCNTs before (C) and after (D) the addition of thiocholine. Images were extracted from a movie taken with a 100 × objective. Scale bars represent 10 µm.

	$(GT)_{15}$ -SWCNT + AChE + ATC	**$(GT)_{15}$ -SWCNT + BChE + ATC**	**$(T)_{30}$ -SWCNT + AChE + ATC**	**$(T)_{30}$ -SWCNT + BChE + ATC**
β	0.6 ± 0.33	0.5 ± 0.07	0.6 ± 0.07	0.6 ± 0.03
$k\ [U \cdot L^{-1}]$	$(4.6 \pm 13.42) \times 10^{-1}$	$(4.3 \pm 2.98) \times 10^{-2}$	$(1.5 \pm 0.82) \times 10^{-1}$	$(1.8 \pm 0.70) \times 10^{-2}$
n	0.50 ± 0.42	1.8 ± 1.92	0.8 ± 0.30	0.9 ± 0.26
$LOD\ [U \cdot L^{-1}]$	0.38	0.06	0.02	0.003

Table S1. Four parameter logistic regression fit parameters, with a zero baseline. Values were extracted by curve fitting using MATLAB and are displayed $\pm$ their 95% confidence interval. $\frac{I-I_0}{I_0} = \beta \frac{x^n}{x^n+k^n}$, where I is the final fluorescence intensity, I_0 is the initial fluorescence intensity, β is a proportion constant equal to the intensity at saturation, k is the inflection point, n is a cooperativity factor, and x is cholinesterase concentration.

	$(GT)_{15}$ -SWCNT + 1:30 FBS + 450 μM ATC	**$(GT)_{15}$ -SWCNT + 1:90 FBS + 450 μM ATC**	**$(GT)_{15}$ -SWCNT + 1:300 FBS + 450 μM ATC**
a	0.34 ± 0.02	0.34 ± 0.04	0.26 ± 0.02
b [min^{-1}]	0.34 ± 0.06	0.18 ± 0.05	0.11 ± 0.02

Table S2. Exponential function fit parameters. Values were extracted by curve fitting to an exponential function using MATLAB and are displayed $\pm$ their 95% confidence interval. $\frac{I-I_0}{I_0} = a \cdot (1 - e^{-b \cdot t})$, where I is the final fluorescence intensity, I_0 is the intensity of the relevant control serum sample without ATC addition, b is the rate constant, a is the saturation value at the long-time limit, and t is the time since ATC addition in minutes.

תקציר

אנזימי כולינאסטראז משתתפים בתהליכים ביוכימיים רבים בגוף, ופעילות אב-נורמלית שלהם מקושרת לפתולוגיות מגוונות כמו מחלות נוירודגנרטיביות וסרטן. בעוד שמעכבי כולינאסטראז מהווים תרופות למחלות כמו אלצהיימר ודמנציה, חשיפה אקוטית למנות גבוהות, שנמצאות בחומרי הדברה וחומרי לחימה כימיים עצביים, יכולה להיות קטלנית. לכן, מדידה של פעילות כולינאסראז חשובה לשימושים רבים, מחיפוש טיפולים חדשים למחלות נוירודגנרטיביות לגילוי בשטח של גורמי סיכון בריאותי פוטנציאליים. בעבודה זו אנו מציגים את הפיתוח של גלאי פלואורסנטי באינפרה אדום, מבוסס ננו צינוריות פחמן, לפעילות כולינאסטראז ומציגים את השימוש שלו למדידת הפעילות והעיכוב של האנזימים אצטליכולינאסטראז ובוטירילכולינאסטראז. אנחנו מוכיחים רגישות גבוהה מ $U\ L^{-1}$, בדומה לשיטת Ellman המקובלת בתחום, ומדגימים קבלת סיגנל פלואורסנטי בתחום 900-1400 ננומטר, החופף לחלון השקיפות הביולוגי. למיטב ידיעתנו, זה סנסור הכולינאסטראז בעל אורך הגל הגבוה ביותר שדווח עד כה בספרות המדעית. סנסור האינפרה-אדום שפיתחנו פותח כיווני מחקר חדשים לגילוי בזמן ובמרחב של פעילות כולינאסטראז ויכול לעזור במחקר שאלות חדשות במערכת הכולינרגית, גילוי בשטח של גורמי סיכון בריאותיים ומדידת ביומרקרים למחלות בזמן אמת בסביבה ביולוגית.

ניטור הפעילות והעיכוב של אנזימי כולינאסטראז באמצעות סנסורים פלורסנטיים מבוססי ננו-צינוריות פחמן

דן לבנטל

הפקולטה למדעים מדויקים על שם ריימונד ובברלי סאקלר, בית הספר לכימיה

אוניברסיטת תל אביב

עבודת גמר לקראת תואר "מוסמך אוניברסיטה" בכימיה פיזיקלית

כ"ד בתשרי, תשפ"ג

העבודה נעשתה במחלקה להנדסה ביו רפואית בהנחיית ד"ר גילי ביסקר

ניטור הפעילות והעיכוב של אנזימי כולינאסטראז באמצעות חיישנים פלורסנטיים מבוססי ננו-צינוריות פחמן

דן לבנטל

הפקולטה למדעים מדויקים על שם ריימונד ובברלי סאקלר, בית הספר לכימיה

אוניברסיטת תל אביב

עבודת גמר לקראת תואר "מוסמך אוניברסיטה" בכימיה פיזיקלית

כ"ד תשרי, תשפ"ג

העבודה נעשתה במחלקה להנדסה ביו רפואית בהנחיית ד"ר גילי ביסקר